

Title:

High Throughput Screening Identifies Novel Pharmacological Inhibitors of Interferon-gamma-induced Nitric Oxide Production, Alleviating Ulcerative Colitis and Bacterial Sepsis in Mice

Introduction:

Interferons, originally discovered to interfere in the process of viral replication, modulate a multitude of biological functions and is involved in disease pathogenesis. They are classified as Type I, Type II, and Type III IFNs. IFN- γ is the only type II IFN structurally unrelated to Type I IFNs. The cellular sources of IFN- γ include CD4⁺ T helper cell type 1 lymphocytes, CD8⁺ cytotoxic lymphocytes, Natural Killer cells, etc. The binding of IFN- γ to its receptor results in the receptor's phosphorylation by JAK, enabling the receptor's SH2 domains to bind to STAT1 for subsequent activation. Phosphorylated STAT1 monomers form a homodimer known as GAF, which gets translocated into the nucleus. GAF binds to the GAS to activate the genes responsible for the primary transcriptional response (*Irf1*, *Irf9*). One of the targets of GAF is IRF1, a transcription factor that binds on ISRE and initiates the secondary transcriptional program of its target genes (*Gbp1*, *Psmb10*). The expression of NOS2 catalyzing the production of NO is one of the key markers in IFN- γ signaling in different cell types, including macrophages and tumors (Rakshit et al., 2014; Ivashkiv, 2018).

NO is a gaseous free radical that mediates intra- and inter-cellular communication to perform essential roles in various physiological processes. NO is produced by a family of enzymes called NOS. There are three isoforms of NOS: nNOS or NOS1, iNOS or NOS2, and eNOS or NOS3. All three isoforms of NOS produce NO by converting the amino acid L-arginine to L-citrulline using oxygen and NADPH as cofactors. *Nos2* is primarily expressed in immune cells such as macrophages and is induced by pro-inflammatory cytokines such as IFN- γ and bacterial products such as LPS (Ignarro, 2019). The catalytic activity of NOS isoforms is regulated by various mechanisms, including calcium/calmodulin binding, phosphorylation, and the availability of

substrate and cofactors. However, the expression of *Nos2* depends on intracellular calcium, but not the catalytic activity of NOS2, facilitating faster action than other NOS isoforms. NO mediates pleiotropic downstream effects and regulates the outcomes of the IFN- γ signaling pathway (Lu et al., 2015).

IFN- γ and other cytokines are involved in many inflammatory disease progression and pathogenesis. For instance, in tuberculosis, the IFN- γ -activation of *Mycobacterium*-infected murine macrophages effectively clears off the infection. These beneficial effects are attributed to the IFN- γ -mediated NO production, following NO-dependent transcriptional activation of antimicrobial pathways, direct microbicidal action, and host cell apoptosis (Herbst et al., 2011; Braverman & Stanley, 2017). The IFN- γ -NO axis also ameliorates other infectious diseases such as leishmaniasis, AIDS, malaria, influenza, COVID-19, etc (Saha et al., 2010; Kak et al., 2018). On the contrary, the NOS2-mediated excessive NO production is associated with poor survival in cancer patients by increasing tumor aggressiveness, e.g., triple-negative breast cancer, *KRAS*-induced lung cancer, and colon adenomas (Ambs et al., 1998; Okayama et al., 2013; Granados-Principal et al., 2015). The IFN- γ -induced NOS2-mediated hyperproduction of NO also imparts detrimental effects in several inflammatory and autoimmune diseases: Inflammatory bowel disease (IBD), Multiple Sclerosis, Rheumatoid arthritis, Systemic lupus erythematosus, encephalomyelitis, Sjogren's syndrome, sepsis, etc (Rafa et al., 2010; Arellano et al., 2015; Benchabane et al., 2016; Dey et al., 2016; Yadav et al., 2018, 2019; Liu et al., 2022).

Chronic inflammatory diseases require maintenance treatment with non-steroidal anti-inflammatory drugs and managing disease exacerbation with steroidal medications. The long-term use of corticosteroid medications often leads to unavoidable adverse effects: steroidal resistance, osteoporosis, myopathy, osteonecrosis, adrenal insufficiency, opportunistic infections, etc. In ulcerative colitis, corticosteroids are used as mainstay treatment to manage flare-ups, yet almost 50% of the patients exhibit steroid resistance (Coates et al., 2021). In addition, the therapeutic benefits of non-steroidal NOS inhibitors to treat inflammatory diseases have been questionable because of their mixed efficacies, adverse side effects, and unintended drug interactions (Warner & McCartney, 1998; Yadav et al., 2019). These problems necessitate identifying alternative non-steroidal anti-inflammatory drugs, potentially targeted to specific inflammatory axes, such as IFN- γ -induced NOS2-mediated hyperproduction of NO. In this study, our approach was to perform high-

throughput screening of the Library of Pharmacologically Active Compounds (LOPAC^{®1280}) in an *in vitro* model of mouse tumor cell line H6 as these cells produce high amounts of IFN- γ -induced NO (Prasanna et al., 2007; Rakshit et al., 2014). We also aimed to triage the hits from the screening, identify leads through validation and test their effects in orthogonal assays. Finally, we extended the assessment of the leads to primary mouse PMs and, more importantly, in the *in vivo* mice inflammatory disease models: dextran sodium sulfate (DSS)-induced ulcerative colitis and *Salmonella* Typhimurium-induced sepsis.

Objectives:

- a.** To identify novel anti-inflammatory compounds inhibiting IFN- γ -induced NO production
- b.** To validate the hits and identify leads
- c.** To characterize the mechanism of action of the leads
- d.** To evaluate the lead compounds in the *in vivo* inflammatory disease models of mice

Materials and Methods

The list of instruments and reagents along with country of origin and catalog numbers are listed in Table 1.

Table 1. Materials

Reagents		
Name	Brand	Catalogue number
1 mL Syringe with 26G needle	BD PrecisionGlide™ (Tuas Avenue 2, Singapore)	303060
10 mL Syringe with 21G needle	BD Discardit™ II (Fraga, Spain)	CE0318
24-well plate, flat bottom	Thermo Scientific (Roskilde, Denmark)	142475
6-well plate, flat bottom	Thermo Scientific (Roskilde, Denmark)	140675
96-well plate, flat bottom	Corning (Kennebunk, ME, USA)	3599
Auranofin	Sigma-Aldrich (St. Louis, MO, USA)	AA6733
Azithromycin dihydrate	Sigma-Aldrich (St. Louis, MO, USA)	PZ0007
Beta mercaptoethanol	Sigma-Aldrich (St. Louis, MO, USA)	M6250-100ML
BIO	Sigma-Aldrich (St. Louis, MO, USA)	B1686
Brewer's Thioglycollate	Himedia (LBS Marg, Mumbai, India)	M019
Chloroform	Sigma-Aldrich (St. Louis, MO, USA)	C2432-4X25ML
DCFDA	Sigma-Aldrich (St. Louis, MO, USA)	D6883
Dextran sodium sulfate	MP Biomedical (Canada)	216011080
Diethyl Pyrocarbonate	Sigma-Aldrich (St. Louis, MO, USA)	D5758-25ML
Dulbecco's Modified Eagle Medium, High Glucose	Himedia (LBS Marg, Mumbai, India)	AT067-10X1L
Dulbecco's Phosphate Buffered Saline	Himedia (LBS Marg, Mumbai, India)	TS1006-10X1L

EDTA	Sigma-Aldrich (St. Louis, MO, USA)	E9884
Ethanol	EMSURE® EMD Millipore (Billerica, MA, USA)	654833
Fetal Bovine Serum	Gibco (Fountain Park, Paisley, UK)	10270106
Gentamicin sulfate	Gbioscience (St. Louis, MO, USA)	AB1022
Glycine	Sigma-Aldrich (St. Louis, MO, USA)	G8898
HCl	SDFCL (Powai, Mumbai, India)	20125L25
IL6 mouse ELISA kit	Invitrogen (V.A.Graiciuno, Vilnius, Lithuania)	88-7064-88
Interferon- γ	PeproTech (Rocky Hill, NJ, USA)	315-05
Isopropyl alcohol	Sigma-Aldrich (St. Louis, MO, USA)	I9030-100ML
L-Glutamine	Himedia (LBS Marg, Mumbai, India)	RM049-25G
LOPAC®1280	Sigma-Aldrich	LO1280
LP44	Sigma-Aldrich (St. Louis, MO, USA)	L9793
Methanol	Qualigens (Powai, Mumbai, India)	Q32407
N-(1-Naphthyl) ethylenediamine dihydrochloride	Sigma-Aldrich (St. Louis, MO, USA)	N-5889
ortho-Phosphoric acid	Sigma-Aldrich (St. Louis, MO, USA)	612162
Paraformaldehyde	Sigma-Aldrich (Bommasandra, Bangalore, India)	158127
PE-conjugated anti-mouse MHC Class I antibody	Ebioscience (San Diego, California, USA)	12-5999-82
Penicillin G Sodium Salt	Himedia (LBS Marg, Mumbai, India)	TC020
Pentamidine isethionate	Sigma-Aldrich (St. Louis, MO, USA)	P0547
RevertAid First Strand cDNA Synthesis kit	Thermo Scientific (V.A.Graiciuno, Vilnius, Lithuania)	K1622
RNase A	Qiagen (Hilden, Germany)	19101
Rolipram	Sigma-Aldrich (St. Louis, MO, USA)	R6520
Ruthenium red	Sigma-Aldrich (St. Louis, MO, USA)	R2751
Sanguinarine chloride	Sigma-Aldrich (St. Louis, MO, USA)	S5890
SDS	Sigma-Aldrich (St. Louis, MO, USA)	L4390
SeaKem® LE Agarose	Lonza (Rockland, ME, USA)	50004-500g
Sodium Azide	Himedia (LBS Marg, Mumbai, India)	RM123
Sodium Bicarbonate	Sigma-Aldrich (St. Louis, MO, USA)	S5761-500g

Sodium chloride	Qualigens (Powai, Mumbai, India)	Q15915
Streptomycin	Gbioscience (St. Louis, MO, USA)	AB1037
Sulfanilamide	Sigma-Aldrich (St. Louis, MO, USA)	S9251-100G
SYBR Green Mix	Gbioscience (St. Louis, MO, USA)	786-5062
TNF- α mouse ELISA kit	Invitrogen (V.A.Graiciuno, Vilnius, Lithuania)	BMS607-3
TRI Reagent®	Sigma-Aldrich (St. Louis, MO, USA)	T9424-100ML
Tris(hydroxymethyl)aminomethane	Sigma-Aldrich (St. Louis, MO, USA)	252859
Trypan Blue solution	Sigma-Aldrich (St. Louis, MO, USA)	T6146-5G
Trypsin-EDTA (0.25% Trypsin, 0.001% EDTA)	Himedia (LBS Marg, Mumbai, India)	TCL-014
Instruments		
Name	Brand	
CFX Connect™	BioRad (Singapore)	
FACSVerse™	BD Biosciences (USA)	
Humidified CO2 Incubator	Sanyo (UK)	
Infinite M200 Pro Multimode Microplate Reader	Tecan (Austria)	
Nanodrop™	Thermofisher Scientific (USA)	
Thermomixer HM100 Pro	DLAB (India)	
Brightfield microscope	Euromex CCCD5 5.0 MP (India)	

Cell culture

H6 (hepatoma), Renca (renal adenocarcinoma), RAW 264.7 (monocyte/macrophage) cell lines, and primary mice PMs were maintained in Dulbecco's modified minimal essential medium-High Glucose (DMEM), with 10% FBS (Prasanna et al., 2007; Rakshit et al., 2014; Chandrasekar et al., 2015). The media was supplemented with 5 μ M β -mercaptoethanol, 100 μ g/ml penicillin, 250 μ g/ml streptomycin, 50 μ g/ml gentamycin, and 2 mM glutamine (hereafter 10% DMEM). The cells were seeded in T75 flasks at 4-5x10³ cells/mL density and maintained at 37°C in a humidified incubator with 5% CO₂ and 95% humidity. The spent cell culture media was replaced with fresh cell culture media after 36-48 hours of growth in these flasks. The cells were passaged

when 70-80% confluency was attained. Cell lines were passaged by treating with Trypsin-EDTA for 2-5 minutes at room temperature, and the reaction was stopped using an equal volume of 10% DMEM. The cells were used for experimentation within passage 1-10. More detailed features of the cell lines used in this study are tabulated in Table 2.

Table 2. Details about the mouse adherent cell lines used in this study

Name	Mouse strain	Tissue origin	Cell type	Immortalization method	Antigen expression	References
H6	A/J	Liver hepatocyte	Hepatoma	Information not available	H-2 ^a	Thompson et al., 1981 ; Monaco et al., 1982
Raw264.7	BALB/c	Ascites	Macrophage	Abelson murine leukemia virus transformed	H-2 ^d	Ralph & Nakoinz, 1977
Renca	BALB/c Cr	Renal cortex	Epithelial, adenocarcinoma	Arose spontaneously	H-2 ^d	Murphy & Hrushesky, 1973

Griess assay for nitrite estimation

The production of NO was estimated from the accumulation of nitrite, the metabolic product of NO metabolism, in the medium using the Griess reagent as described previously ([Malu et al., 2003](#)). NO has very short half-life and gets oxidized to nitrite and nitrate. Nitrite is estimated as a surrogate to measure the NO production.

Briefly, 25 µL of the cell free supernatant, 25 µL of 10% DMEM, and 100 µL of Griess reagent {a mixture of 1% (w/v) Sulfanilamide and 0.1% (w/v) N-(1-Naphthyl) ethylenediamine dihydrochloride prepared in 2.5% phosphoric acid} were mixed and subsequently, absorbance was

measured at 550 nm using a microtiter plate reader (Molecular Devices, Downingtown, PA, USA). The amount of nitrite in the supernatants was calculated using a standard curve performed using 1.22–625 μM of sodium nitrite.

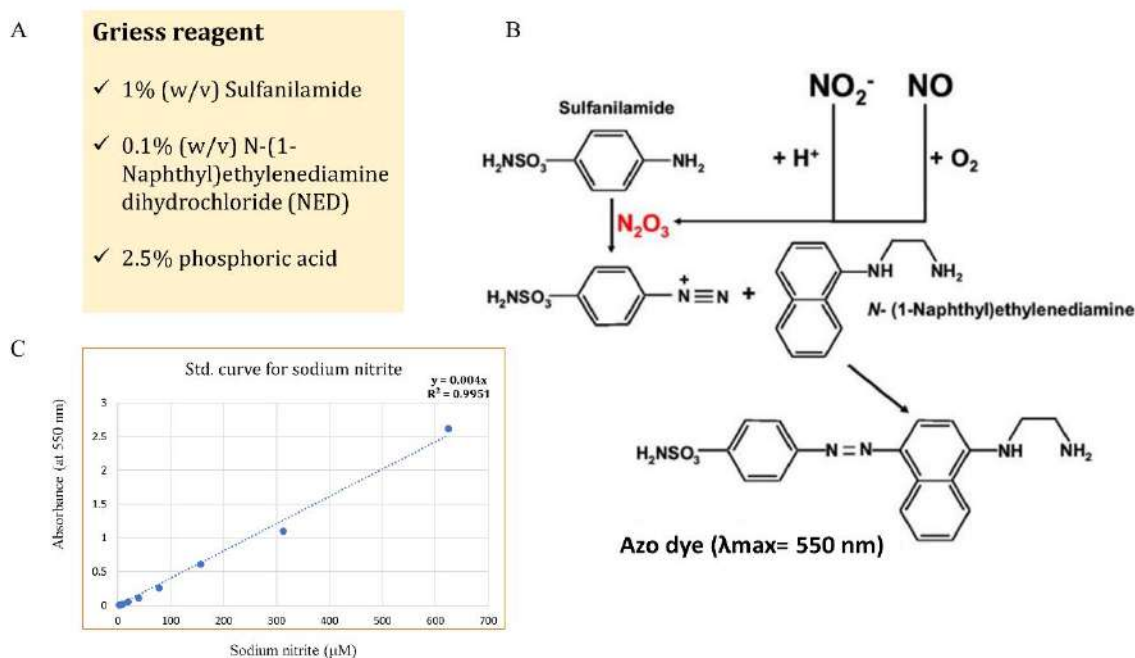


Fig.1. Griess assay

Components of the Griess reagent (A). The chemical reaction of the Griess assay is described as follows. The nitrosating agent dinitrogen trioxide (N_2O_3) generated from acidified nitrite (or from the autoxidation of NO) reacts with sulfanilamide to yield a diazonium derivative. This reactive intermediate will interact with N-1-naphthylethelene diamine to yield a colored diazo product that absorbs strongly at 550 nm (B). The standard curve was prepared using sodium nitrite and measurement of absorbance at 550 nm (C).

Trypan blue dye exclusion assay

Trypan blue dye exclusion assay was performed to assay for percentage change in cell number (Rakshit et al., 2014). Briefly, logarithmically growing cells were seeded at an initial density of 1×10^4 cells per well in a 96-well plate (0.15×10^6 cells per well for peritoneal exudate cells). The cells were treated with IFN- γ and compounds as indicated for 24 h. Adherent cells were harvested by adding 0.5% Trypsin-EDTA per well. The cell suspension was mixed with an equal volume of 0.4% Trypan blue, and the number of live cells was counted in a hemocytometer.

$$\% \text{Cell number} = \frac{(\text{Number of live cells in the treated set}) \times 100}{\text{Number of live cells in control}}$$

Compound library

The Library of Pharmacologically Active Compounds (hereafter named LOPAC^{®1280}) is a library of 1,280 off-patent small molecules. This biologically annotated collection of compounds is a set of pharmaceutically relevant structures that impact most signaling pathways and covers all major drug target classes. Several compounds are approved (FDA, EMA, and other drug regulatory bodies) and marketed drugs. The compounds are arranged in 96-well format in 16 racks of 80 and provided at a concentration of 10 mM in absolute DMSO.

LOPAC^{®1280} screening on H6 cells

On the day before the experiment, H6 mouse hepatoma cells were seeded at a density of $\sim 1 \times 10^4$ cells/well of 96-well plates in 10% DMEM. The cells were maintained at 37°C in a humidified incubator (Sanyo, UK) with 5% CO₂ for 8-12 hours. The compounds were then diluted to treat the H6 cells. DMSO was toxic for H6 cells above 1% of the final solvent concentration. Therefore, the DMSO-induced-cytotoxic effect was eliminated by diluting all compounds in 10% DMEM to reduce DMSO solvent final concentration to 0.1%. The compounds were assayed in biological duplicates at 10 μ M. The H6 cells were pre-incubated with the compounds for 15 minutes, followed by IFN- γ treatment and incubation for 24 hours to identify the ones that reduced NO production. IFN- γ was added into all wells at a final concentration of 10 U/mL except in those labeled: 'Control,' 'LNMA,' and 'DMSO control.' LNMA was used at 250 μ M. 0.5% DMSO was

added in 'DMSO control.' The H6 cells were incubated at 37°C in a humidified incubator with 5% CO₂ for 24 hours. The cell-free supernatant was collected for Griess assay for nitrite estimation.

Counter screening for cytotoxicity

We speculated that some acute leads might be compounds that impart cytotoxic effects at 10 µM. This is because stressed or dead cells might not have optimal conditions to form NO, and therefore, the assigned test compounds might qualify the cut-off score as leads. To mitigate this, a counter-screen for cytotoxicity was performed with the proceeding of the primary screen. The wells were selected by sorting less than 70% inhibition of nitrite formation and visual examination of the cytomorphology under a standard light microscope at (×20) magnification. The damaged cytomorphology might be caused due to the loss of structural integrity and blebbing. Therefore, these compounds interfered with the assay used in the primary screen. The wells with altered cytomorphology than the untreated cells were assayed for Trypan Blue Dye exclusion. Any compound that reduced the percent change in cell number > 30 was considered toxic.

Data analysis and selection of hits

The mean difference in nitrite concentrations upon compound treatment compared to IFN-γ was z-score transformed on GraphPad Prism software version 8.0.2. The dataset was transformed into a p-value using the normal cumulative distribution function of the z-score in the Microsoft Excel version 2211 and ranked based on the p-value. The q-values were derived from the rank and p-value using the 'MIN' function. The compounds with q-value < 0.5 (or z-score < -1.9) were assigned as hits and considered putative leads. The toxic hits identified in the counter screening for cytotoxicity were eliminated.

IC₅₀ Determination

The compounds were tested in 2-fold serial dilutions to inhibit nitrite production using Griess assay. The concentration ranges of the compounds tested are as follows: pentamidine isethionate (7.8-1250 nM), azithromycin dihydrate (1.25-40 µM), rolipram (0.0078-40 µM), auranofin (7.8-

1000 nM), BIO, sanguinarine chloride, LP44, thapsigargin (7.8-500 nM), and ruthenium red (1.25-80 μ M). Such concentration ranges were chosen to avoid toxic upper limits exceeding the CC₉₀. The dataset was transformed into the log scale for logarithmic interpolation. The maximal inhibitory response of the compounds was normalized to 0%. The non-linear regression fit was applied to calculate the IC₅₀ value ranges and goodness of fit R² value.

Flow cytometry (ROS, MHC class 1)

The intracellular ROS estimation and surface staining of MHC class 1 were performed as previously described (Rakshit et al., 2014). Briefly, H6 cells were cultured in 6-well plates at a density of 3×10^5 cells per well and treated with IFN- γ . The intracellular ROS was estimated by incubating the cells with 10 μ M DCFDA dye at 37°C water bath for 30 mins in the dark. Cell pellets were resuspended in 200 μ L of PBS in all three cases. Cell surface staining for MHC class 1 was performed by incubating the cells in the blocking buffer {5% FBS and 0.1% (w/v) sodium azide in PBS} for 30 min. The cells were stained with the PE-conjugated anti-MHC Class 1 antibody at the dilution 1:300 for 30 mins with intermittent tapping. The cells were fixed with 4% paraformaldehyde. Data acquisition was performed in the BD FACSVerse™ flow cytometer and analyzed using BD FlowJo™ (BD Biosciences US).

Primer designing

Oligonucleotide primers were designed using the NCBI Primer-Blast tool. First, the gene name and '*Mus musculus*' were input in the NCBI search bar. The option of Refseq transcripts was clicked to obtain the nucleotide sequence of mRNA in FASTA format. The option of 'pick primers' was clicked to reach the NCBI Primer-Blast window. The PCR product size was selected 100-250 bp range. Primer melting temperature (T_m) was selected in the range of 59-63°C (optimum 61°C). The primer search was set, allowing them to amplify all splice variants.

IDT OligoAnalyzer™ tool was set at the qPCR parameter to analyze the GC content (preferably 40-60%), melting temperature (preferably 61-63°C), identification of hairpin structure potential, homodimerization, and heterodimerization of the oligonucleotide sequences. Identifying any

oligonucleotide interactions in the primer pair for hairpin structure, homodimerization, and heterodimerization with ΔG less than -4 kcal/mol was considered excluded. The list of Primers for RT-qPCR analysis is mentioned in the **Table 3**.

Table 3. List of RT-qPCR primers

Gene name	Forward Primer	Reverse Primer
<i>Actb</i>	TGCTTCTAGGCGGACTGTTAC	TTTGGGAGGGTGAGGGACTT
<i>Cd274</i>	CCCTTGACAGCTACTGCCTC	GGTTCGGCTATGCTCGTCTT
<i>Gapdh</i>	AGGTCGGTGTGAACGGATTG	TGTAGACCATGTAGTTGAGGTCA
<i>Hprt1</i>	GTTGGGCTTACCTCACTGCT	TAATCACGACGCTGGGACTG
<i>Irf1</i>	ATGCCAATCACTCGAATGCG	TTGTATCGGCCTGTGTGAATG
<i>Nos2</i>	GTTCTCAGCCCAACAATAACAAGA	GTGGACGGGTCGATGTCAC
<i>Socs1</i>	TCTCGCTCCTTGGGGTCTGT	CCCCAATAGAAGCCGCAGG
<i>Tap2</i>	GGACCCAATGGATCAGGGAA	TTGACAGAACCCGAGAACAGC

Reconstitution of the oligonucleotide primers

The lyophilized Oligonucleotide vials were centrifuged at 15000 g for 10 minutes. To prepare a 100 μ M stock, nuclease-free water was added at the recommended volume provided on the technical datasheet. The vials were gently tapped and centrifuged at 130 g (pulse). The vials were kept at 56°C for 20 min and agitated intermittently after every 5 min. A pulse of 13,300 g was given 1-2 times. A 10 μ M working solution was prepared in nuclease-free microfuge tubes. The primers were stored at -20°C till further usage.

RNA isolation, reverse transcription and RT-qPCR

The methods of RNA isolation, reverse transcription and RT-qPCR were performed with minor modifications (Prasanna et al., 2007; Ray et al., 2019). H6 cells were seeded in 6-well plates at a density of 3 x 10⁵ cells per well. The cells were maintained at 37 °C in a humidified incubator (Sanyo, UK) with 5% CO₂ overnight. The media was replaced the next day, and cells were treated with IFN- γ (10 U/mL) and pharmacological agents as indicated. The culture media was removed, and the cells were washed once with 1X PBS. 1ml TRI reagent was added immediately in each

well of the 6-well plate and mixed vigorously using a P1000 micropipette. The cell lysates were stored in microfuge tubes at -80°C till further processing. The samples were thawed at 4°C and vortexed in a Thermomixer at 30°C and 1500 RPM for 30 minutes. After that, 300 µL of chloroform was added and mixed vigorously for 1 minute and then undisturbed for 5 minutes at room temperature. The tubes were centrifuged at 12000 g for 20 minutes at 4°C. The aqueous phase was carefully collected, and 200 µL of chloroform was added. The centrifugation and aqueous phase collection were repeated once. 500 µL of isopropanol was added to the aqueous phase collected and kept at -20°C overnight. The mixture was centrifuged at 14500 g for 30 minutes at 4°C. The supernatant was discarded, and the pellet was dislodged in 1 mL of 70% ethanol. The tubes were centrifuged at 12000 g for 10 minutes at 4°C. The washing and centrifugation steps were repeated. The residual 70% ethanol was discarded, and the pellet was kept at room temperature for 30 minutes for drying. The pellet was then dissolved in 20 µL of nuclease-free water. The concentration and quality of isolated RNA were measured in a NanoDrop spectrophotometer. Further, the quality of RNA samples was assessed by running the samples on a 1% agarose gel electrophoresis. The residual trace amounts of DNA in the RNA samples were digested with DNase I (Table 4).

The DNase I digestion mixture was prepared as tabulated in Table 4. The RNA samples with DNase I digestion mixture were incubated at 37°C for 30 min. 2 µl of 50 mM EDTA was added to stop the DNase I reaction, spun the contents in the tubes, and incubated at 65°C for 10 min to inactivate the DNase I enzyme. The quality of RNA samples after DNase I digestion was assessed by running the samples on a 1% agarose gel electrophoresis.

Table 4. DNase I digestion recipe

Component	Volume
RNA	3-4 µg
10x Reaction Buffer	2 µl
DNase I, RNase free (#EN0521)	1 µl
Ribolock RNase inhibitor (20 U/µl)	0.5 µl
Nuclease-free Water (DEPC-treated)	Adjusted according to RNA sample volume

Total	20 μ l
-------	------------

The mRNA from 1-3 μ g total RNA was reverse transcribed to cDNA using a first-strand cDNA synthesis kit (Table 5).

Table 5. Reaction mixture of first strand cDNA synthesis

The tabulated components were mixed in the indicated order in ice. The first strand cDNA synthesis was performed at 42°C for 60 min. The reaction was terminated by heating the samples at 70°C for 5 min. The cDNA samples were stored at -20°C before use.

Components	Volume
5x Reaction Buffer	4 μ l
Ribolock RNase inhibitor (20 U/ μ l)	1 μ l
10 mM dNTP Mix	2 μ l
RevertAid RT (200 U/ μ l)	1 μ l
Oligo(dT) Primer (100 μ M)	1 μ l
Template RNA	(0.1 ng – 5 μ g) 11 μ l
Total	20 μ l

The cDNA samples were mixed gently and spun briefly. The cDNA samples were diluted at 1:20 in nuclease-free water for PCR amplification. RT-qPCR was performed in accordance with Minimum Information for Publication of Quantitative Real-Time PCR Experiments (MIQE) guidelines ([Bustin et al., 2010](#); [Taylor & Mrkusich, 2014](#)). A master mix of the following reagents was prepared for each gene, along with the cDNA template, as mentioned in **Table 6**. In a 96-well plate (Bio-Rad), the master mix with the cDNA template was loaded. The plate was centrifuged at 1500 RPM for 2-3 minutes to settle any content onto the inside walls of the wells. The qPCR was performed in a thermal cycler with a heated lid.

Table 6. Reaction mixture for RT-qPCR

Components	Volume
SYBR green	5 μ l
Forward primer	0.25 μ l

Reverse primer	0.25 μ l
Template	4.5 μ l
Total	10 μ l

RT-qPCR was performed with the following program: initial denaturation (95°C for 10 minutes), denaturation (95°C for 10 seconds), annealing (57°C for 30 seconds), and extension (70°C for 20 seconds). The denaturation to extension steps was repeated for 39 cycles.

PCR primer efficiencies are crucial for correct results analysis. For the calculation of gene expression, such as the $\Delta\Delta C_t$, the PCR primer efficiencies are assumed to be comparable for the gene of interest and the reference gene. Dissimilar PCR primer efficiencies within the experiment can impact the result. Therefore, the primer sets used in the experiments were tested to determine whether they lie between 90 – 110% efficiency and were chosen for the experimentation (Svec et al., 2015).

Hprt1, *Gapdh* and *Actb* genes were tested for the suitability of usage as the reference gene. *Gapdh* transcription was differentially regulated upon IFN- γ -activation in H6 cells, however, the *Actb* and *Hprt1* transcript levels remained comparable. The C_t values of gene expression data were transformed to $2^{-\Delta\Delta C_t}$ using *Actb* as the reference gene. The data quality was assessed by examining the melt curve.

ELISA

IL6, TNF- α , and IL1 β amounts in cell-free culture supernatants or sera were estimated using eBioscience™ ELISA Ready-SET-Go™ kit, per manufacturer's instructions (Pathak et al., 2021). Briefly, sera or cell-free culture supernatants were incubated in wells of a 96 well-plate coated with capture antibodies against the cytokines mentioned above for 2 h at room temperature. The plates were then washed with PBS with 0.05% Tween-20 (PBS-T) and incubated with biotinylated detection antibodies for 1 h at room temperature. The detection antibodies were conjugated with Streptavidin-HRP by incubating the plates at room temperature for 30 min in dark. The plates were then washed with PBS-T and treated with 3,3',5,5'-Tetramethylbenzidine for 2-5 min. The reaction was stopped using 2N H₂SO₄. Absorbance was measured at 450 nm.

Cell cycle profiling

Flow cytometry-based cell cycle profiling was performed as previously described (Prasanna et al., 2007; Chattopadhyay et al., 2023), the cells were immediately fixed with a gentle vortex using ice-cold 70% ethanol. The intracellular RNA was digested by treating the cell suspension with 100 µg/mL RNase A for 30 mins at room temperature. The cell suspension was stained with 50 µg/mL propidium iodide for 30 mins at room temperature in the dark.

Cheminformatics-based prediction of the compound targets

Molinspiration (version 2022.08) and SWISSTargetPrediction (version ChEMBL23) cheminformatics tools were used to predict the bioactivity and target proteins of the compounds (<https://www.molinspiration.com>). The SMILES of the compounds were input to derive the results.

Brightfield microscopy

~10⁴ H6 cells were seeded on 96-well plates and treated with or without IFN-γ. Images were captured after 24 hours of treatment under a 40X objective lens, fitted in a brightfield microscope.

Animals and genotyping

The *Nos2*^{-/-} mice were acquired from National Institute of Immunology, New Delhi, India. The mice were bred and maintained in the Central Animal Facility at the Indian Institute of Science (Bangalore, India). Genotyping of the *Nos2*^{-/-} mice was performed as previously described (Truett 2000; Yadav et al., 2018). Briefly, ~2 mm of the tail tip of the C57BL/6 WT and *Nos2*^{-/-} mice were collected into microfuge tubes. 75ul 25mM NaOH / 0.2 mM EDTA was added and heated at 95°C for 1 hour. The temperature was reduced to 15°C. 75ul of 40 mM Tris HCl (pH 5.5) was added into the lysate and centrifuged at 100g for 3 mins. The DNA concentration in the supernatant was estimated using NanoDrop. PCR was performed with ~30-50 ng of total DNA. The primer sequences are mentioned in the supplementary Table 7. The PCR program was as follows: initial

denaturation (96°C, 10 mins), denaturation (96°C, 30 seconds), annealing (57°C, 30 seconds), extension (72°C, 30 seconds) and final extension (72°C, 10 mins). The steps from denaturation to extension were repeated 39 times. The PCR product was run on 1.5% agarose gel electrophoresis.

Table 7. Primers used in *Nos2*^{-/-} genotyping

Name	Sequence (5' - 3')
<i>Wild type</i>	TCAACATCTCCTGGTGGGAAC
<i>Forward mutant</i>	ACATGCAGAATGAGTACCGG
<i>Reverse mutant</i>	AATATGCGAAGTGGACCTCG

Peritoneal macrophage (PM) harvesting from mice

PMs were harvested from mice as previous mention ([Chandrasekar et al., 2015](#); [Chattopadhyay et al., 2023](#)). Briefly, C57BL/6 mice were bred and housed at a specific pathogen-free facility at the Central Animal Facility at the Indian Institute of Science (Bangalore, India). Six-to-eight-week-old male mice with body weights ranging from 20 to 25 grams were used for all experiments. 4% Brewer's thioglycollate broth was prepared, autoclaved, and aged for at least 1 month before use. Mice were euthanized 96 h after i.p. injection of 1 ml of 4% Brewer's thioglycollate to collect TG-elicited macrophages. Resident peritoneal macrophages were collected without the injection of Brewer's thioglycollate.

Peritoneal cells were harvested by peritoneal lavage with 10% DMEM, counted using a hemocytometer, and seeded in a 96-well plate at a density of 0.15x10⁶ cells per well. The non-adherent cells were washed away after 1 hour of seeding. The Institutional Animal Ethics Committee approved all procedures (IAEC) constituted per article number 13 of the CPCSEA rules laid down by the Government of India (IAEC approval number: CAF/ethics/805/2021).

***In vivo* DSS-induced ulcerative colitis and *Salmonella* Typhimurium-induced sepsis**

DSS-induced ulcerative colitis was induced in mice, as previously described (Pathak et al., 2021). Colitis was induced by administering 2% (w/v) DSS in drinking water for seven consecutive days (starting from day 0). The mice were monitored for changes in body weight, stool consistency, and hematochezia. The disease activity index (DAI) was scored daily as described previously (Park et al., 2015). The scoring criteria is tabulated in **Table 8**.

Table 8. DAI scoring system

DAI = (score of weight loss) + (score of stool consistency) + (Hematochezia)

Hematochezia is the presence of gross blood in the stool or anus

Loose stool is the form of stool that readily becomes paste on anus of mice

Score	Weight loss (%)	Stool consistency	Hematochezia
0	None	Normal	Absent
1	0-10	-	-
2	11-15	Loose stool	-
3	16-20	-	-
4	>20	Diarrhea	Present

The 20% reduction in the body weight change was considered the humane endpoint. To test the role of immune nitric oxide, *Nos2*^{-/-} mice were compared with C57BL/6 mice by dividing them into groups (n = 3-6 each): untreated control and colitic for WT and *Nos2*^{-/-}. To test the effect of leads *in vivo*, mice were randomly divided into several groups (n = 3-7 each): vehicle control, colitis, and the colitis groups receiving the lead compounds. The lead compounds were intraperitoneally injected at 10 mg/kg on day 2 and day 4. On day 7, animals were sacrificed, and the endpoint analyses were performed.

In the case of sepsis, BALB/c mice were injected intraperitoneally with 2-5 x 10⁶ CFU of *Salmonella* Typhimurium bacterial culture grown for 3-5 hr. Each condition consisted of 6 male mice aged 6-8 weeks and a body weight of 22-24 g (Chattopadhyay et al., 2022). The compounds

were injected intraperitoneally 3-4 hours post-infection with pentamidine (1 and 10 mg/Kg) or auranofin (0.3 and 1 mg/Kg). The survival of the mice was monitored until 72 hours post-infection.

The essential information concerning ARRIVE guidelines is in **Table 9**.

Table 9. Ten essential information from ARRIVE guidelines for mice experiments

Essential Item	Description
Study design	<p>In the case of DSS-induced colitis, the groups being compared were untreated, DSS-treated, pentamidine or azithromycin or rolipram or auranofin administration, along with DSS-treatment.</p> <p>In the case of <i>Salmonella</i> Typhimurium-induced sepsis, the groups being compared were untreated, <i>Salmonella</i> Typhimurium-injection i.p., and pentamidine or auranofin administration upon <i>Salmonella</i> Typhimurium-injection i.p. The test compounds are well-studied, and some are FDA-approved drugs. Therefore, Compound-alone controls were not included. Each mouse was considered an experimental unit.</p>
Sample size	<p>The sample size was determined, as discussed in the article by Dell et al., 2002 (Dell et al., 2002). Center for Biomath, Dept. of Peds, CUMC was used to estimate sample size based on the following primary outcome measures. The mouse model of DSS-induced colitis accounted for the colon length reduction and disease activity index (Pathak et al., 2021).</p> <p>The median survival of the mice was accounted for in the mouse model of <i>Salmonella</i> Typhimurium-induced sepsis (Yadav et al., 2018). It yielded that ≤ 6 mice are sufficient to perform the statistical comparisons to test compound effects in both pre-clinical mice disease models.</p>
Inclusion and exclusion criteria	<p>All animals in the experiment were included as data points in the analysis. The exact value of the number of mice for each examination is mentioned in the figure legends.</p>
Randomization	<p>The mice were allocated to each experimental group using simple randomization without stratification. The potential confounders, such as the treatment order or measurements, were not controlled.</p>

Blinding/Masking	The lead investigators involved in the measurements of disease pathogenesis parameters in mice were blinded to the group allocation at the different stages of the experiment.
Outcome measures	<p>In the case of DSS-induced mouse colitis, the outcome measures were as follows: body weight change, stool consistency, rectal bleeding, colon length, and serum cytokine. A 20-25% body weight reduction was considered a humane endpoint.</p> <p>In the case of <i>Salmonella</i> Typhimurium-induced sepsis in mice, the hour of mice survival was the only outcome measure. The humane endpoint was the persistence of lethargy, hunched posture, reluctance to move, and unsteady gait for more than 12 hours.</p>
Statistical methods	The statistical methods of each analysis are mentioned in the article's figure legends and materials and methods section.
Experimental animals	6-8 weeks old male C57BL/6 or <i>Nos2</i> ^{-/-} mice ranging in body weight between 18-25 g were incorporated into the experiment.
Experimental procedures	The section of materials and methods describes the testing procedure, such as the dosage of the compounds administered, route of administration, and the CFU of <i>Salmonella</i> Typhimurium injected.
Results	The results section describes the outcomes.

The Institutional Animal Ethics Committee approved all procedures (IAEC) constituted per article number 13 of the CPCSEA rules laid down by the Government of India (CAF/ethics/805/2021).

Results

Primary Screen for Inhibition of IFN- γ -induced NO Production

Our previous studies demonstrated that IFN- γ leads to NO formation in several mice cell lines *in vitro*. The IFN- γ also activates transcriptional programs that can be categorized as NO-dependent and NO-independent pathways and the former lead to the blockade of cell cycle progression and induction of apoptosis (Prasanna et al., 2007; Rakshit et al., 2014). The *in vitro* model of IFN- γ -activation of H6 cells was utilized to perform the primary screening to identify novel pharmacological modulators of IFN- γ -induced nitrite production using the Griess assay (Fig.2A). First, we standardized the optimal conditions to conduct the large-scale screening, including the seeding density of H6 cells, concentration of IFN- γ , and the time-point for the end-point assay. The seeding density of H6 hepatoma cells was selected to be 1×10^4 cells in each well because it attained 60-70% confluency after 8 hours of seeding. H6 cells produced nitrite in the concentration-dependent manner of IFN- γ . IFN- γ at 10 U/mL produced saturating amounts of nitrite after 24 hours of incubation. The IFN- γ activation also reduced the percent change in cell number in a concentration-dependent manner (Fig.2B, C; Fig.3A). The assay signal dynamic range and data variation at the specified conditions were measured as screening window coefficient or Z'-factor (Zhang et al., 1999). The Z'-factor was calculated to be 0.49, indicating that the separation band is small but suitable for identifying leads.

For the primary screen, H6 cells were pre-treated with compounds from the LOPAC^{®1280} (Sigma) for 15 minutes, followed by IFN- γ treatment and incubation for 24 hours to identify compounds that reduced NO production. The assay design is depicted in Figure 3.1B and the plate-wise performance report of the positive controls from the primary screening is illustrated as a heatmap (Fig.3C). The plate setup and full modulation profile of IFN- γ -induced NO production is represented (Fig.2D, E). Lowered nitrite could be due to cell death caused by the toxicity of some compounds. Our counter screening for cytotoxicity identified 22 compounds that imparted cytotoxic effects (Table 10).

The mean difference of nitrite concentration between IFN- γ alone positive control and all the duplicate test compounds were z-score transformed. The z-scores were used to calculate the p-

value and q-values. The compounds with $q\text{-value} < 0.5$ (or $z\text{-score} < -1.9$) were assigned as putative leads. A negative Z-score indicates the inhibition of nitrite formation.

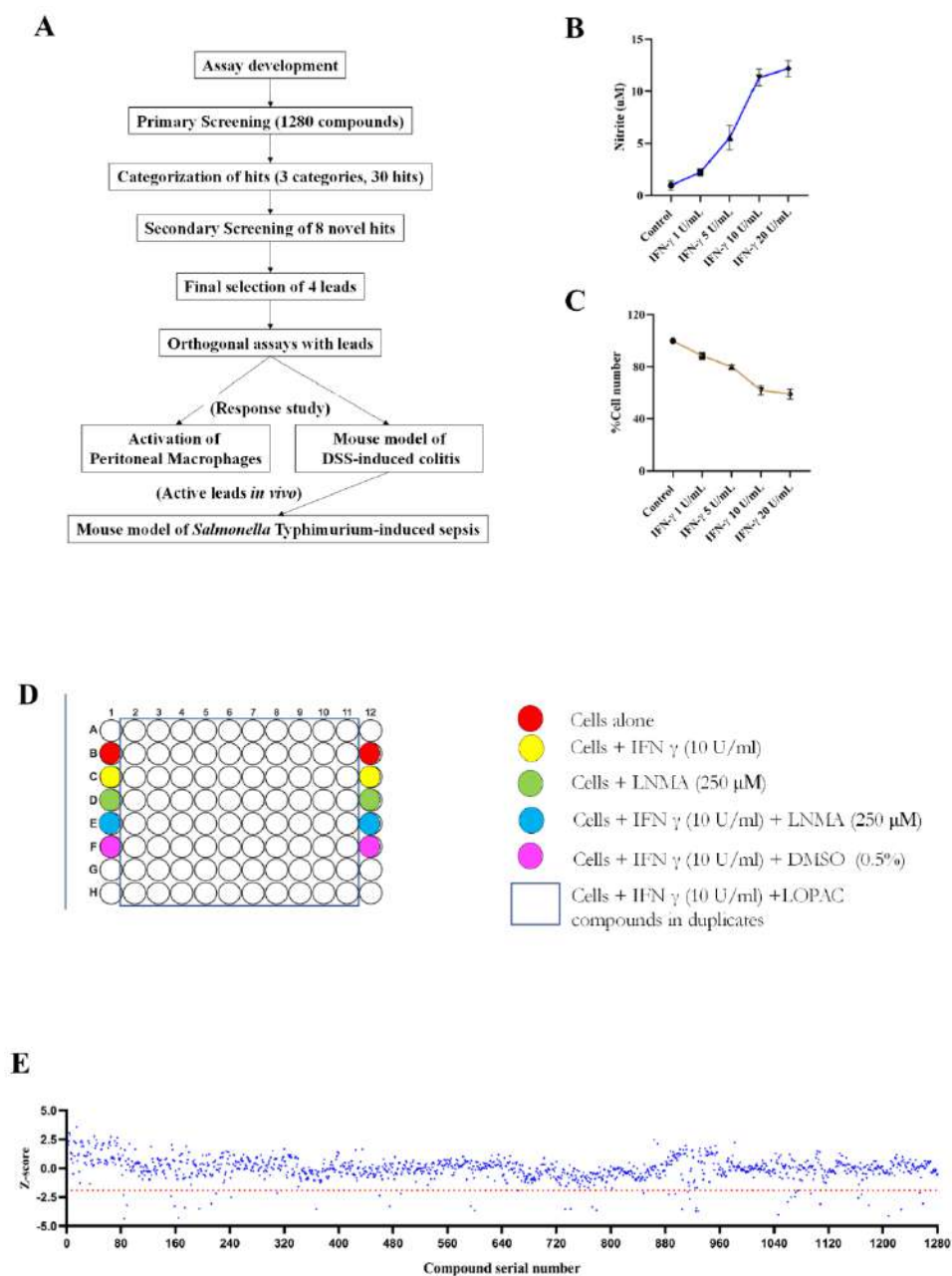


Fig.2. Primary Screening of LOPAC^{®1280} in H6 hepatoma cell line for pharmacological inhibitors of IFN- γ -induced NO production.

Large-library screening and downstream assays pipeline for the identification of pharmacological inhibitors of IFN- γ -induced NO production and anti-inflammatory effects (A). Concentration-dependent response of H6 hepatoma cells to IFN- γ with respect to nitrite production (B) and percent cell number change (C) after 24 hours. The data representative of 3-4 independent experiments (B-C). The map of the 96-well plate used in the process of primary screening (D). Screening of 1280 pharmacologically active compounds from LOPAC^{®1280} was performed in the 96-well plate. The H6 hepatoma cells were seeded at a density of 1×10^4 cells/well and allowed to adhere for 6-8 hours. The cell culture media was replaced with a fresh one to remove the floating cells. The cells were pre-treated with compounds for 15 minutes and treated with 10 U/mL of IFN- γ for 24 hours. The dot plot represents the data distribution. The dotted line in red represents the threshold for positive lead compounds. Numbers on the x-axis represent the serial numbers of the location of the compounds across 16 plates (E). Each data point is representative of mean + SD from 3 independent experiments. Each independent experiment involved a pair of biological replicates in 96-well plates. The measurements were recorded in technical duplicates (B, C).

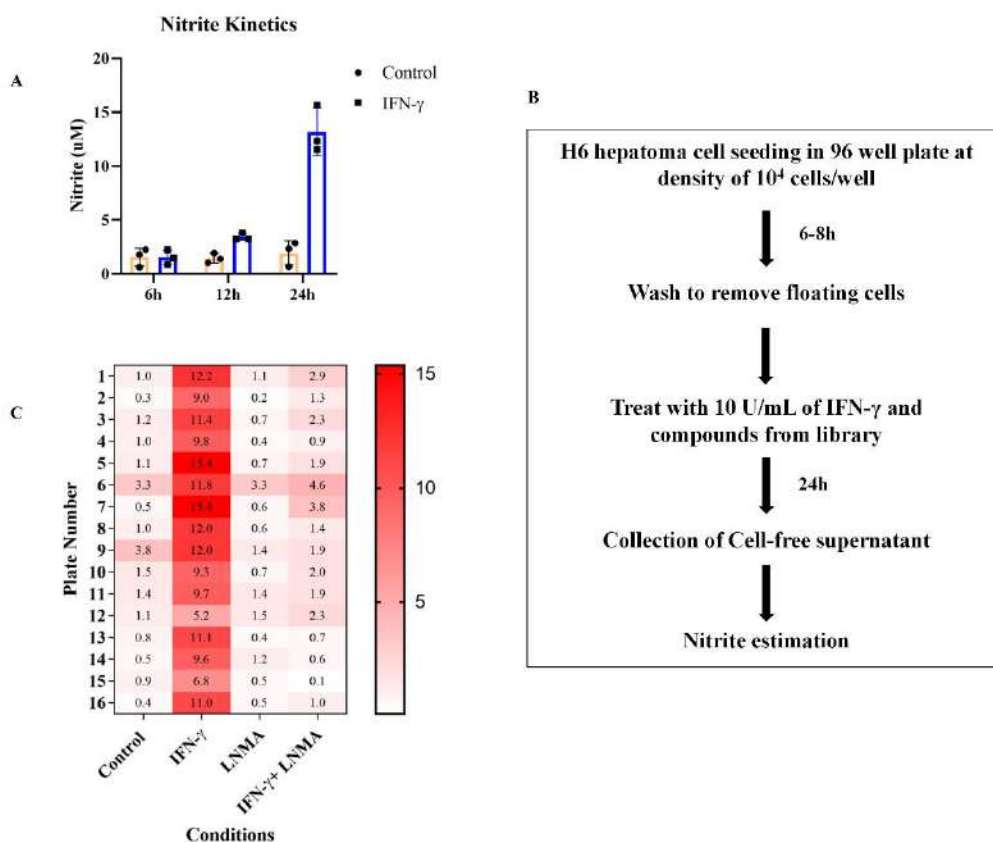


Fig.3. Assay design and performance profile of the primary screening.

The kinetic profiling of nitrite production in response to IFN- γ in H6 cells (A). A graphical representation of the assay design to perform the primary screening (B). The H6 hepatoma cells were expanded in T75 flask at 37°C and 5% atmospheric CO₂. The cells were trypsinized at 70-80% confluence, seeded in 96-well plate at a density of 10⁴ cells in each well, and incubated for 8-10 hours. The cell-culture supernatant was replaced with fresh DMEM supplemented with 10% FBS to remove floating cells. The cells were pre-treated with the compounds from LOPAC® 1280 at 10 μ M final concentration for 15 minutes. Subsequently, IFN- γ was added at final concentration of 10 U/mL. The cell-free supernatant was harvested after 24 hours of incubation at 37°C and 5% atmospheric CO₂. The colorimetric Griess assay was performed to estimate the level of Nitrite in the cell-free supernatant (B). The performance of the positive and negative controls for each plate is depicted in the heatmap. The plate number is assigned in the column-wise manner. The values in each square represents the mean value from the technical duplicates. The color gradient scale in the heatmap represents the amounts of nitrite produced in μ M. Each datapoint is representative of independent experiment (A).

Table 10. Cytotoxic compounds in the LOPAC®1280 screening

S.N o.	Plate S.No. (LOPAC® 1280)	Name	Class	Selectivity	Z-score	p-value	q-value
1	164	Brefeldin A from <i>Penicillium brefeldianum</i>	Cytoskeleton and ECM	Golgi apparatus	-4.32	7.79E-06	0.004985
2	1208	Vincristine sulfate	Cytoskeleton and ECM	Tubulin	-4.12	1.82E-05	0.007752
3	928	Podophyllotoxin	Cytoskeleton and ECM		-3.69	0.000109	0.021544

4	600	Idarubicin	DNA Metabolism		- 3.6 4	0.0001 34	0.0215 44
5	779	Mitoxantrone	DNA Metabolism		- 3.6 3	0.0001 41	0.0215 44
6	1227	Vinblastine sulfate salt	Cytoskeleton and ECM	Tubulin	- 3.5 6	0.0001 79	0.0215 44
7	905	Topotecan hydrochloride hydrate	Apoptosis and Cell Cycle	topoisomer ase I	- 3.5 4	0.0001 93	0.0215 44
8	733	Nocodazole	Cytoskeleton and ECM	beta- tubulin	- 3.5 4	0.0001 93	0.0215 44
9	367	Diphenyleneiodo nium chloride	Nitric Oxide	eNOS	- 3.5 3	0.0002 05	0.0215 44
10	741	CHM-1 hydrate	Apoptosis		- 3.5 1	0.0002 19	0.0215 44
11	195	Gemcitabine hydrochloride	Apoptosis and Cell Cycle		- 3.4 9	0.0002 36	0.0215 44
12	475	AC-93253 iodide	Hormone	RAR(a)	- 3.2 7	0.0005 2	0.0336 33
13	1259	SCH 58261	Purinoceptor	alpha2A	- 3.0 5	0.0011 29	0.0578 1

14	1060	PD-166285 hydrate	Kinase/Phosphatase	Src, FGFR	- 2.9 3	0.0016 75	0.0824 38
15	154	Amsacrine hydrochloride	DNA Repair	TopoII	- 2.4 4	0.0072 04	0.2881 58
16	460	Emetine dihydrochloride hydrate	Apoptosis		- 2.3 6	0.0090 24	0.3500 33
17	310	Colchicine	Cytoskeleton and ECM	Tubulin	- 2.1 5	0.0154 72	0.4715 18
18	341	(S)-(+)-Camptothecin	Apoptosis	TopoI	- 1.5 8	0.0566 4	0.8992 78
19	531	Ellipticine	Cell Cycle	CYP1A1 / TopoII	- 1.4 3	0.0753 46	0.8992 78
20	34	Aminopterin	Antibiotic	Dihydrofolate reductase	- 1.3 3	0.0901 78	0.8992 78
21	536	5-Fluorouracil	Cell Cycle	Thymidylate synthetase	- 0.9 3	0.1749 51	0.8992 78
22	1112	Rotenone	Cell Stress	Mitochondria	- 0.8 7	0.1912 5	0.8992 78

Categorization and Secondary Screen for the Validation of hits

The selected hits were categorized into known NOS inhibitors, steroidal compounds, and novel hits. The compounds in each category are listed in Table 11. Steroidal compounds are well-known for their global anti-inflammatory effects and are known to suppress IFN- γ signaling (Hu et al., 2003; Barnes, 2006). The presence of known NOS inhibitors and steroidal compounds indicated that the primary screening successfully identified the inhibitors of NO production.

Table 11. Categorization of the top hits

Plate S.No. (LOPAC®1280)	Name	Class	Selectivity	Z-score	p-value	q value
Category 1: NOS inhibitors						
85	(±)-AMT hydrochloride	Nitric Oxide	iNOS	-4.36	6.44E-06	0.004985
491	S-Ethylisothiurea hydrobromide	Nitric Oxide	NOS	-2.20	0.013647	0.45249
848	NG-Nitro-L-arginine methyl ester hydrochloride	Nitric Oxide	NOS	-2.17	0.014886	0.464734
Category 2: Steroidal compounds						
174	Budesonide	Hormone	Cortisol	-3.40	0.000325	0.026014
159	Beclomethasone	Hormone	Glucocorticoid	-3.27	0.000525	0.033633
594	Hydrocortisone	Hormone	Cortisol	-3.27	0.000526	0.033633
1179	Triamcinolone	Hormone	Glucocorticoid	-3.20	0.000669	0.04032
213	Betamethasone	Hormone	Glucocorticoid	-3.07	0.001051	0.056027
895	Progesterone	Hormone	Progesterone	-2.22	0.013029	0.450729
220	Corticosterone	Hormone	Glucocorticoid	-2.18	0.014365	0.459682
Category 3: Novel hits						
1046	Auranofin	Phosphorylation	(Not listed)	-4.02	2.89E-05	0.009245
925	Pentamidine isethionate	Glutamate	NMDA	-3.69	0.000109	0.021544

926	LP44	Serotonin	5-HT7	-3.45	0.000278	0.023763
773	BIO	Phosphorylation	GSK-3alpha/beta	-3.35	0.000402	0.030266
89	Azithromycin dihydrate	Immune Cell Signaling	50S subunit	-3.19	0.000693	0.04032
1108	Sanguinarine chloride	Ion Pump	Na ⁺ /K ⁺ ATPase	-3.10	0.000945	0.052585
916	Picrotoxin	GABA	GABA-C	-2.66	0.003865	0.18323
1164	Tetraethylthiuram disulfide	Biochemistry	Alcohol Dehydrogenase	-2.57	0.004955	0.226517
242	Cyclosporin A	Phosphorylation	Calcineurin phosphatase	-2.51	0.005981	0.263186
1065	SB-366791	Vanilloid	VR1	-2.50	0.006168	0.263186
1071	Ruthenium red	Ion Pump	Mitochondrial uniporter	-2.47	0.006606	0.272782
84	Adenosine 3',5'-cyclic monophosphate	Phosphorylation	PKA	-2.33	0.009742	0.366747
885	(±)-Octoclothebin maleate	Dopamine	D2	-2.26	0.011707	0.418331
1169	BAY 61-3606 hydrochloride hydrate	Phosphorylation	Tyrosine kinase	-2.26	0.011766	0.418331
1094	Sobuzoxane	Gene Regulation	Topo II	-2.20	0.013787	0.45249
1254	Tyrphostin A9	Phosphorylation	PDGFR	-2.12	0.016668	0.496155
1072	Rolipram	Cyclic Nucleotides	PDE IV	-2.09	0.018176	0.528754
913	Sodium Oxamate	Biochemistry	Lactate Dehydrogenase	-2.02	0.021671	0.616418

664	p-Iodoclonidine hydrochloride	Adrenoceptor	alpha2	-1.93	0.026573	0.73477
1075	7,8- Dihydroxyflavone hydrate	Cytokines, Growth Factors and Hormones	TrkB	-1.92	0.02698	0.73477

We proceeded with the novel hits to identify compounds that were truly active against IFN- γ -induced nitrite formation and eliminate the false positives. The top six novel hits were auranofin, pentamidine, LP44, BIO, azithromycin and sanguinarine chloride. A few more compounds among the top twenty were tested in a concentration-response assay in the H6 hepatoma cell line. Cyclosporine, ruthenium red, LP44, and thapsigargin failed to fit the regression analysis, implying that these were false positives (data not shown). All other selected hits were fit in the curve, and the nonlinear regression curves were generated (Fig.4). Finally, the lead compounds were chosen based on the R^2 values > 0.7 . The goodness of fit in descending order were: auranofin, azithromycin, rolipram, and pentamidine (Fig.4). The level of nitrite formation was reduced maximally in auranofin treatment, followed by rolipram, azithromycin, pentamidine (Fig.5A).

Dexamethasone was assayed in parallel because this glucocorticoid can represent the steroidal compounds in the list of hits and is a robust positive control to inhibit IFN- γ signaling (Barnes, 2006). Dexamethasone showed the best fit in reducing the IFN- γ -induced NO production with the lowest IC_{50} value range of 6.7-8.1 nM and the best R^2 value of 0.97. This indicated that the concentration-dependent assay for secondary screen was suitable for the selection of the leads (Fig.6).

IFN- γ activation also leads to a reduction in percent change in cell number due to its blocking effects on the cell cycle and induction of apoptosis. It could be argued that the inhibitory effects of the hits could be due to further reduction in cell number. This was tested in the presence of the lead compounds upon IFN- γ treatment in a concentration-dependent manner using Trypan blue dye exclusion. Azithromycin did not affect the cell number reduction. Other lead compounds:

pentamidine, rolipram and auranofin significantly rescued the IFN- γ -induced reduction in cell number (Fig.5B).

To rule out that the effects of top four leads was not specific to H6 cell line-specific, these were tested in RAW 264.7 (monocyte/macrophage) and Renca (renal adenocarcinoma) mouse cell lines. These cell lines were selected because they phenocopy H6 cells by producing NO upon IFN- γ activation. All the leads except azithromycin significantly reduced the formation of IFN- γ -induced NO in the RAW 264.7 cell line. Similarly, all the leads except rolipram reduced the formation of IFN- γ -induced NO in the Renca cell line (Fig.7). In addition, pentamidine rescued the IFN- γ -induced reduction in percent change in cell number in both RAW 264.7 and Renca cell lines. Azithromycin showed similar effect in Renca cell line (Fig.8). Overall, this indicates that the effects observed were not cell-specific.

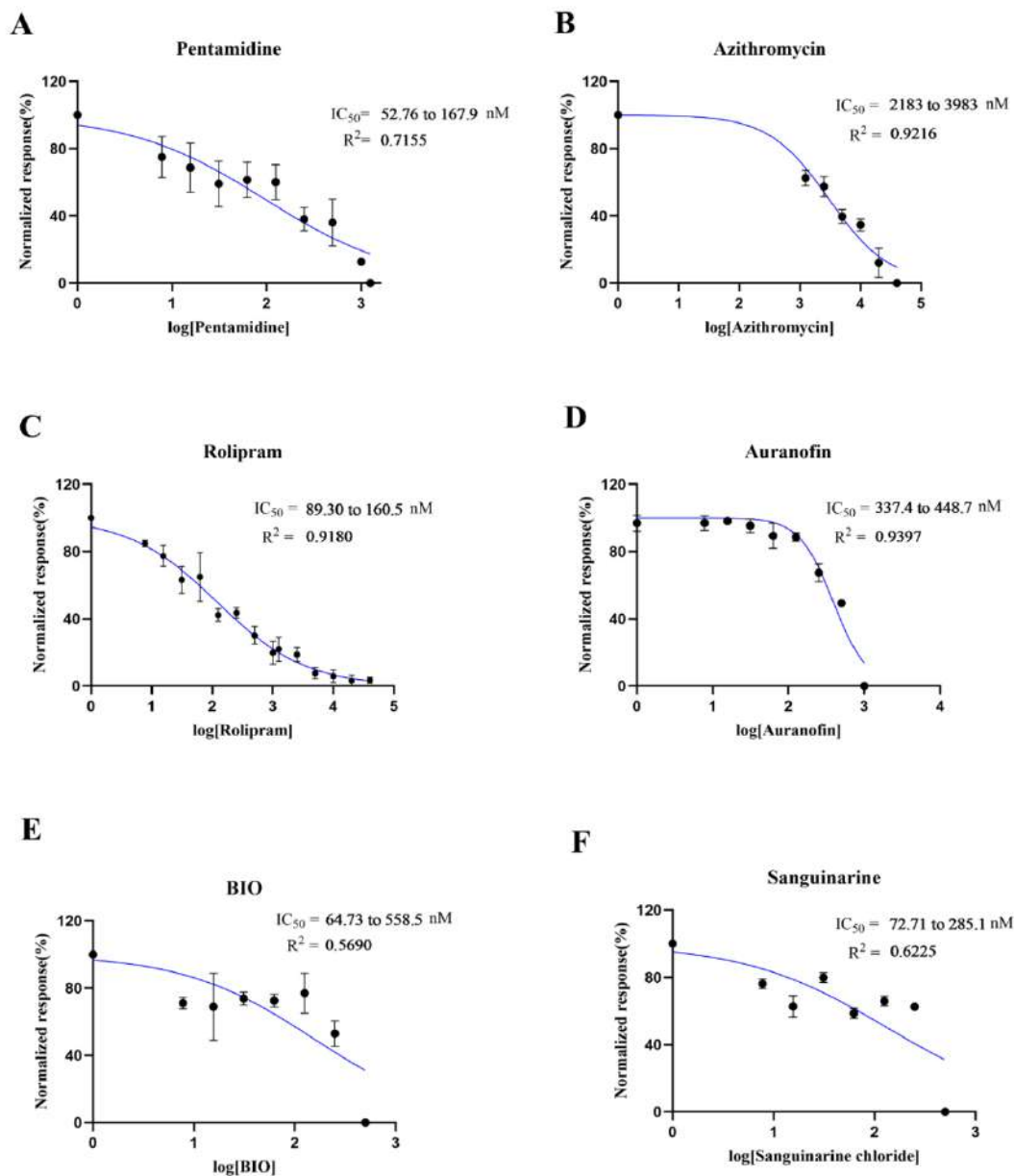


Fig.4. Dose response curves of selected lead compounds.

The concentrations of compounds are presented in log scale and dose response curves were generated using GraphPad Prism software. The IC_{50} value (50% inhibition) range was calculated on the profile likelihood of 95% confidence interval. R^2 value is represented as the goodness of fit. Each datapoint is representative of mean \pm SD from 3 independent experiments. Each independent experiment involved a pair of biological replicates in 96-well plates. The measurements were recorded in technical duplicates.

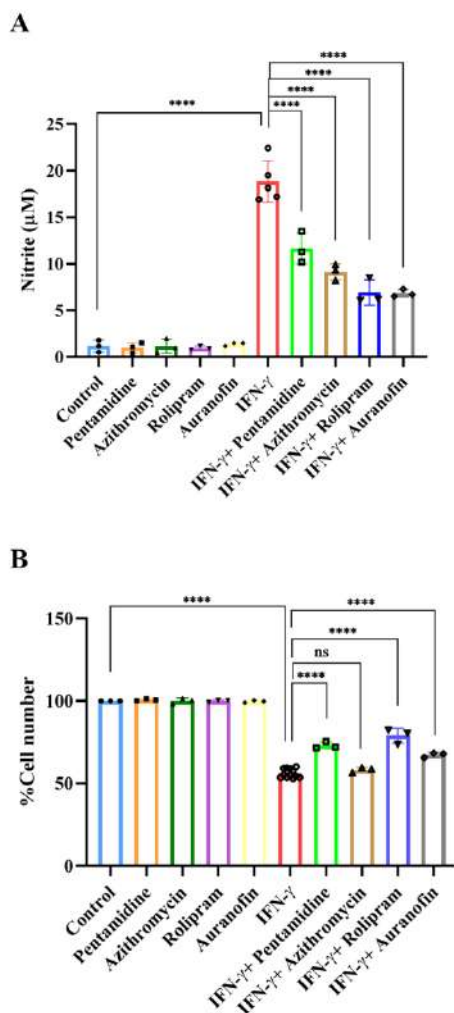


Fig.5. The lead compounds significantly reduce nitrite production

H6 hepatoma cells were seeded at the density of 1×10^4 cells in each well of 96-well plate. Following ~8 hours of incubation, the cell culture supernatant was removed to get rid of dead or non-adherent cells. The cells were co-treated with IFN- γ and the lead compounds: Pentamidine (1 μ M), Azithromycin (40 μ M), Rolipram (10 μ M) and Auranofin (1 μ M). The concentration of nitrite in cell-free supernatant was estimated (A). The percent cell number was measured using Trypan blue dye exclusion assay (B). The statistical analyses were performed using ordinary One-way ANOVA with Sidak's multiple comparisons test. (ns), (*), (**), (***), (****) indicate non-significant difference and the statistical differences of $p < 0.05$, $p < 0.01$, $p < 0.001$, and $p < 0.0001$ between the comparable indicated. Each datapoint is representative of mean \pm SD from independent experiments. Each independent experiment involved a pair of biological replicates in 96-well plates. The measurements were recorded in technical duplicates.

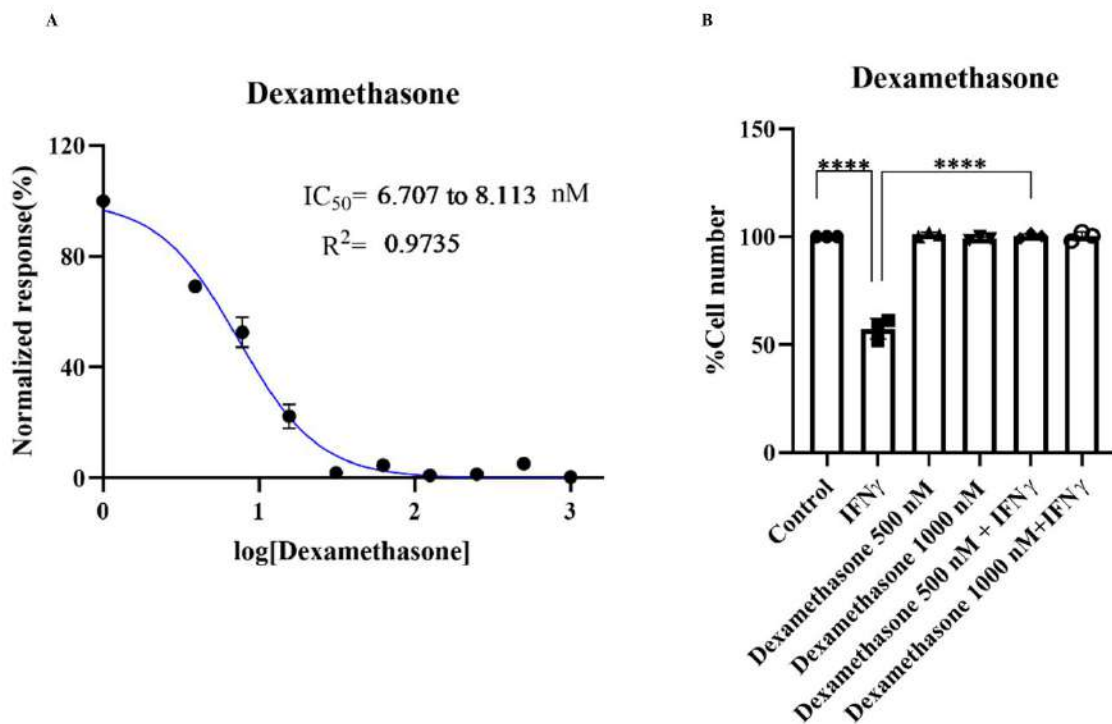


Fig.6. Dexamethasone, a representative of steroidal compounds, is the most potent in dampening IFN- γ -induced nitrite formation and cell number reduction.

Dexamethasone was used as positive control to assay its effects in IFN- γ -induced NO production (A) and %cell number (B). Dexamethasone concentrations are presented in log scale for logarithmic interpolation. The dose response curve was generated using GraphPad Prism software (A). The statistical analyses were performed using ordinary One-way ANOVA with Sidak's multiple comparisons test (B-H). (ns), (*), (**), (***), (****) indicate non-significant difference and the statistical differences of $p < 0.05$, $p < 0.01$, $p < 0.001$, and $p < 0.0001$ between the comparable indicated. Each datapoint is representative of independent experiment. Each independent experiment involved a pair of biological replicates in 96-well plates. The measurements were recorded in technical duplicates.

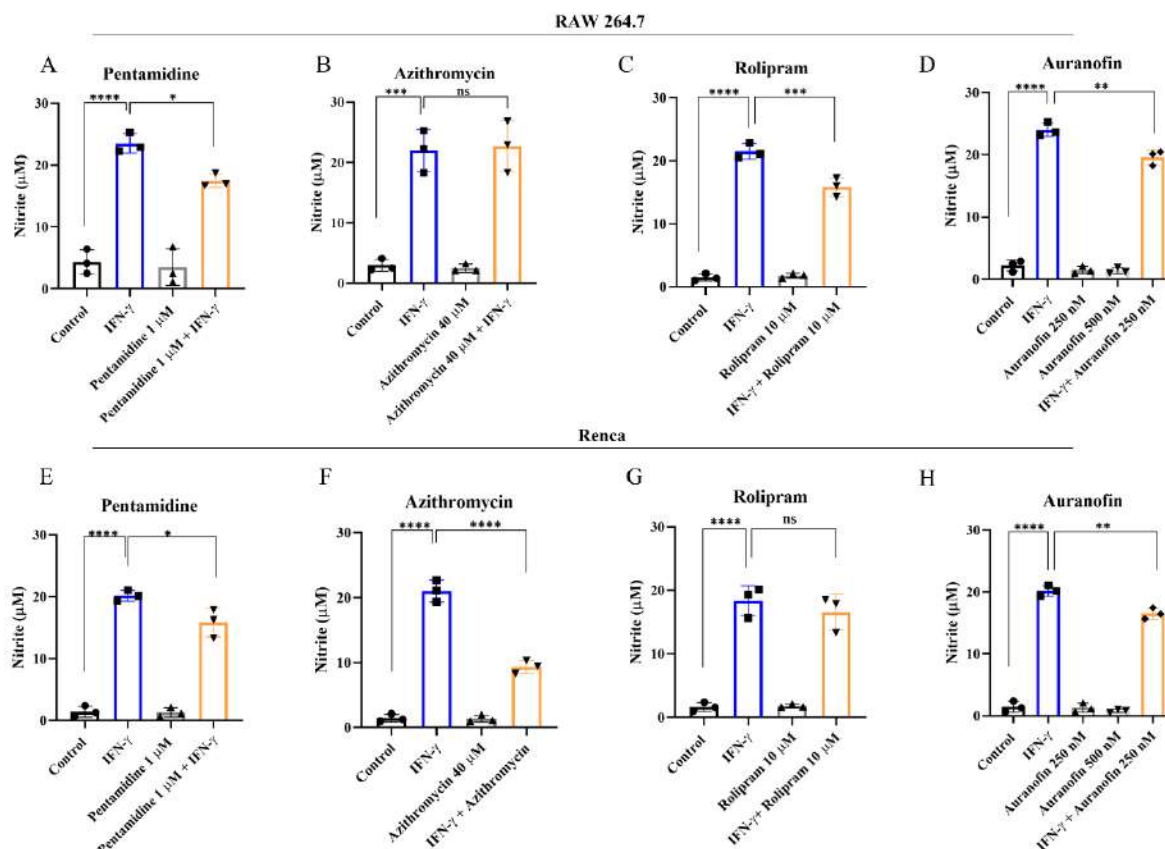


Fig.7. Pentamidine isethionate and auranofin reduces nitrite in both RAW 264.7 and Renca cell lines.

RAW 264.7 and Renca cells were plated at a density of 1×10^4 cells per well in 96-well plate. The cells were co-treated with IFN- γ and the lead compounds: Pentamidine isethionate (1 μ M), Azithromycin dihydrate (40 μ M), Rolipram (10 μ M) and Auranofin (1 μ M). Griess assay for nitrite production was performed after 24 hours of incubation. The statistical analyses were performed using ordinary One-way ANOVA with Sidak's multiple comparisons test. (ns), (*), (**), (***), (****) indicate non-significant difference and the statistical differences of $p < 0.05$, $p < 0.01$, $p < 0.001$, and $p < 0.0001$ between the comparable indicated. Each datapoint is representative of independent experiment. Each independent experiment involved a pair of biological replicates in 96-well plates. The measurements were recorded in technical duplicates.

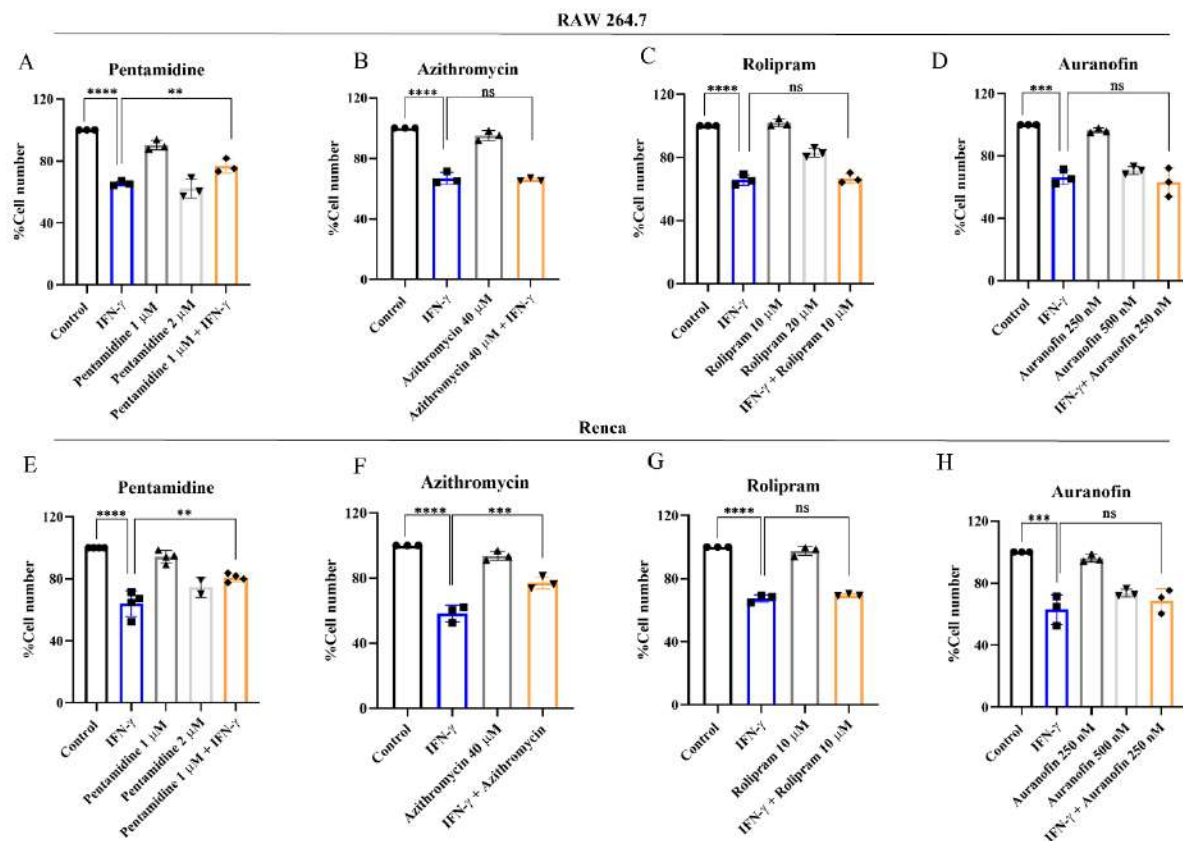


Fig.8. Pentamidine isethionate rescues IFN- γ -induced cell number reduction in both RAW 264.7 and Renca cell lines.

RAW 264.7 and Renca cells were plated at a density of 1×10^4 cells per well in 96-well plate. The cells were co-treated with IFN- γ and the lead compounds: Pentamidine isethionate (1 μ M), Azithromycin dihydrate (40 μ M), Rolipram (10 μ M) and Auranofin (1 μ M). Trypan blue dye exclusion assay to score for percent change in cell number was performed after 24 hours of incubation. The statistical analyses were performed using ordinary One-way ANOVA with Sidak's multiple comparisons test. (ns), (*), (**), (***), (****) indicate non-significant difference and the statistical differences of $p < 0.05$, $p < 0.01$, $p < 0.001$, and $p < 0.0001$ between the comparable indicated. Each datapoint is representative of independent experiment. Each independent experiment involved a pair of biological replicates in 96-well plates. The measurements were recorded in technical duplicates.

Orthogonal Assays to Deduce Plausible Mechanism

The biological response of IFN- γ requires a complex network of multiple signaling pathways. IFN- γ canonically activates the JAK-STAT pathway to induce the expression of transcription factors. These hierarchically activate a cascade of primary response by STAT1, then the secondary response by IRF1, and so on. The NO-independent transcriptional program includes the induction of inflammatory genes, notably *Irf1* (Interferon regulatory factor 1), *Socs1* (suppressor of signal), *Tap2* (antigen processing), and *Cd274* (encodes PD-L1, suppressing immune response). Seminal research on the mechanism of IFN- γ -induced *Nos2* transcription in macrophage cell lines demonstrated that the phosphorylation cascade in the JAK-STAT pathway involving JAK2, MEK1/2, Erk1/Erk2, and STAT1 α are vital players in the process (Blanchette et al., 2003). The transcription factors like IRF1 and NF- κ B, activated in the primary response of IFN- γ , are also crucial binding factors upon the *Nos2* promoter to initiate transcription. The *Nos2* transcription is driven by several transcription factors synergistically (Martin et al., 1994; Blanchette et al., 2003; Saha et al., 2010). Although the precise mechanism in the H6 hepatoma cell line is unknown, the primary processes behind IFN- γ -induced *Nos2* transcription are expected to be broadly similar. The transcriptional program of *Nos2* (Nitric Oxide Synthase 2 in NO production) upon IFN- γ -activation in H6 cells is NO-dependent (Prasanna et al., 2007). The effects of the top four compounds from orthogonal assays in transcriptional activation of IFN- γ -activated H6 cells was evaluated for the genes mentioned earlier. Furthermore, the influence of the compounds on the surface expression of MHC Class 1 and intracellular ROS production in IFN- γ -activated H6 cells was studied using flow cytometry.

To test the transcriptional response, H6 cells were incubated with the leads in the presence of IFN- γ for 12 hours. Expectedly, a significant induction of *Irf1*, *Tap2*, and *Cd274* genes was observed upon IFN- γ activation compared to untreated control. The expression of *Socs1* remained unaffected. None of the lead compounds significantly affected IFN- γ -induced *Irf1* or transcription. The IFN- γ -inducible transcription of *Tap2* and *Cd274* was significantly upregulated in the presence of rolipram but unaffected by other compounds. Except for pentamidine, all the lead compounds significantly downregulated the IFN- γ -induced transcription of *Nos2* (Fig.9).

To understand whether the altered transcription profile affected the surface expression of MHC Class I and intracellular ROS, the compounds-treated IFN- γ -activated H6 cells were subjected to

flow cytometric analysis. None of the compounds was found to affect the IFN- γ -induced surface expression of MHC Class I. However, all compounds significantly reduced the IFN- γ -induced enhanced level of intracellular ROS (Fig.10).

The excessive production of IFN- γ -induced NO leads to the blockade of cell cycle progression (Prasanna et al., 2007). This is presumably due to erroneous DNA replication in the presence of NO-mediated oxidative stress. Therefore, a flow-based cell cycle analysis was performed to obtain a detailed insight into the functional effects of the compounds on H6 cell cycle arrest mediated by IFN- γ signaling. The propidium iodide staining provided a quantitatively comparable measurement of the intracellular DNA content. IFN- γ activation led to a significant increase in the S phase population, indicating an arrest of the cell cycle at the G₂-M checkpoint. Consequently, IFN- γ -activation significantly reduced the G₂-M population. None of the compounds significantly increased the sub-G₁ phase population, indicating no remarkable toxicity leading to DNA damage. Pentamidine showed no distinguishable effect on IFN- γ -induced cell cycle alterations. Rolipram significantly increased IFN- γ -mediated reduction in G₂-M cells. Azithromycin, rolipram and auranofin significantly rescued the IFN- γ -induced arrest of cells at the S phase (Fig.11).

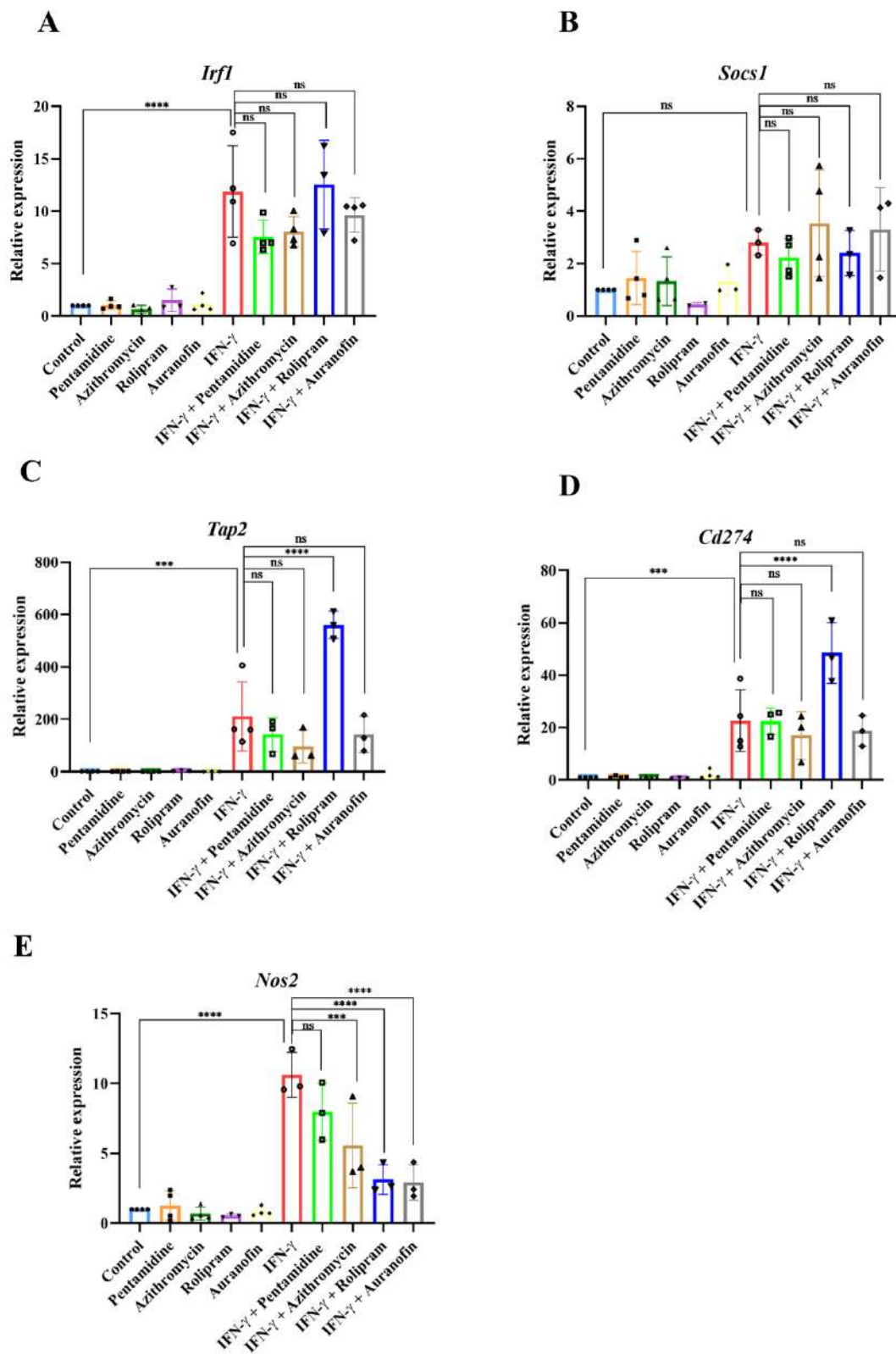


Fig.9. RT-qPCR-based profiling of the modulation of IFN- γ -induced transcriptional program in response to lead compounds.

H6 hepatoma cells were seeded at the density of 3×10^5 cells in each well of 6-well plate. Following ~8 hours of incubation, the cell culture supernatant was removed to get rid of dead or non-adherent cells. The cells were co-treated with IFN- γ and the lead compounds: Pentamidine (1 μ M), Azithromycin (40 μ M), Rolipram (10 μ M) and Auranofin (1 μ M). The RNA was isolated after 12 hours of treatment and reverse transcribed for qPCR analysis of the genes *Irf1* (A), *Nos2* (B), *Tap2* (C), *Cybb* (D), *Cd274* (E), and *Socs1* (F). *Actb* was used as reference gene for determining the $2^{-\Delta C_t}$. The $2^{-\Delta\Delta C_t}$ was determined from untreated controls and denoted as relative expression. The statistical analyses were performed using ordinary One-way ANOVA with Sidak's multiple comparisons test. (ns), (*), (**), (***), (****) indicate non-significant difference and the statistical differences of $p < 0.05$, $p < 0.01$, $p < 0.001$, and $p < 0.0001$ between the comparable indicated. The data is representative of 3-4 independent experiments. Each independent experiment represents a biological replicate performed in a 6-well plate. The measurements of the Cq values were recorded in technical triplicates.

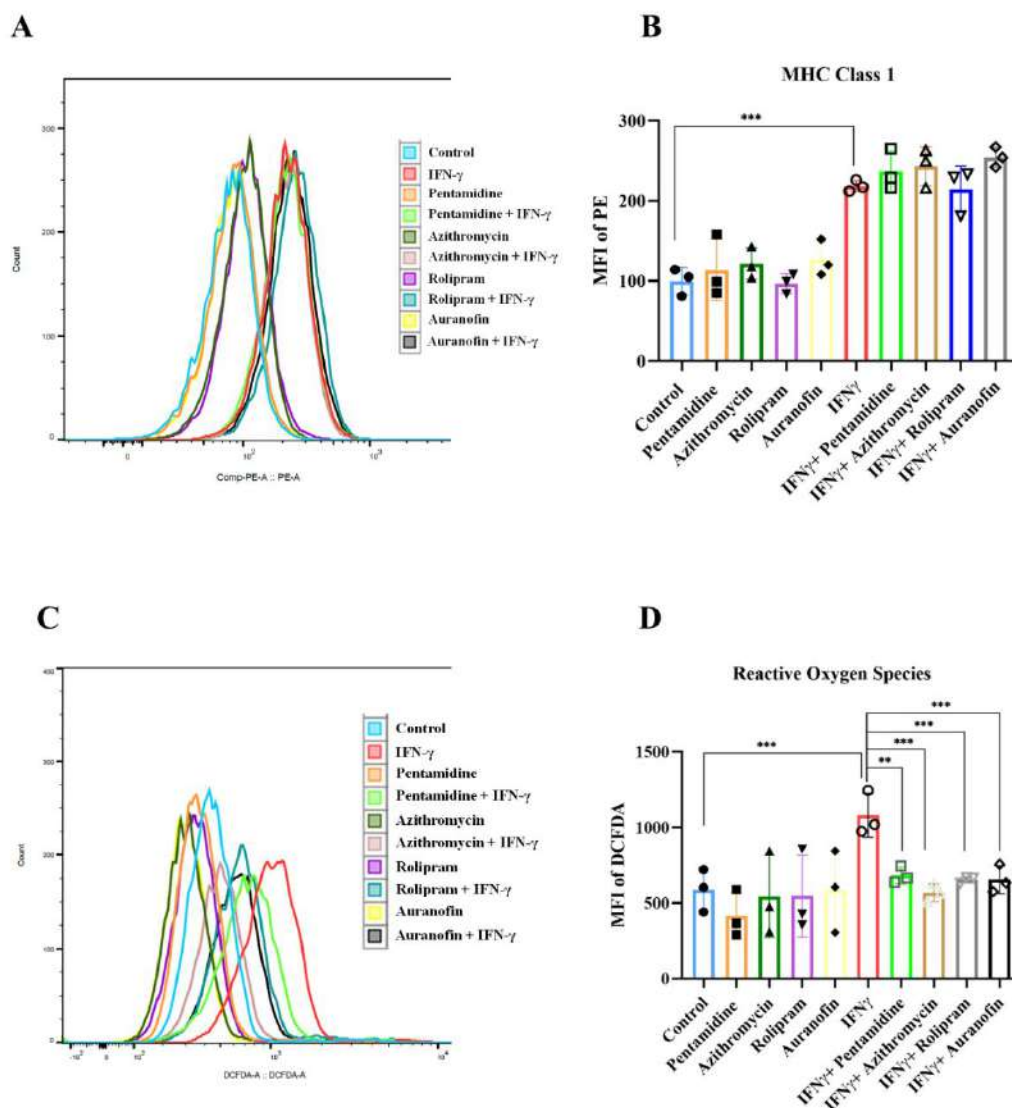


Fig.10. The lead compounds lower IFN- γ -induced ROS formation without affecting surface expression of MHC class 1.

The surface expression of MHC Class 1 (A, B) and intracellular level of ROS (C, D) were enumerated using flow cytometry in H6 cells. The lead compounds: pentamidine (1 μ M), azithromycin (40 μ M), rolipram (10 μ M), and auranofin (1 μ M) were cotreated with IFN- γ for 24 hours prior to the analysis. The statistical analyses were performed using ordinary One-way ANOVA with Sidak's multiple comparisons test (B-H). (ns), (*), (**), (***), (****) indicate non-significant difference and the statistical differences of $p < 0.05$, $p < 0.01$, $p < 0.001$, and $p < 0.0001$ between the comparable indicated. Data is represented as mean \pm SD of 3 independent experiments, each datapoint in the graph representing an independent experiment. Each independent experiment represents a biological replicate performed in a 6-well plate. (B, D).

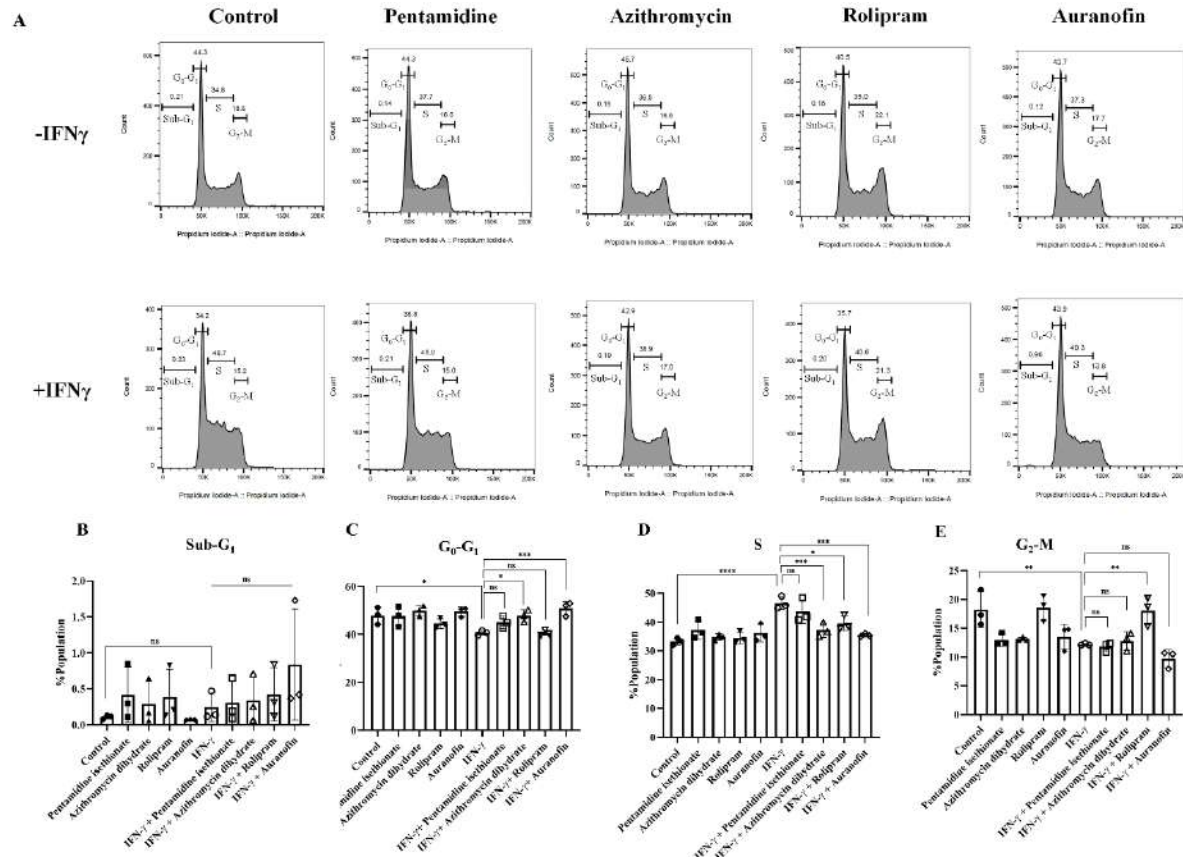


Fig.11. Azithromycin, rolipram and auranofin rescue IFN- γ -activated blockade of H6 cells in S phase.

H6 cells were co-treated with IFN- γ and lead compounds: Pentamidine isethionate (1 μ M), Azithromycin dihydrate (40 μ M), Rolipram (10 μ M), and Auranofin (1 μ M), for 24 hours. The cells were stained with Propidium Iodide for enumerating the intracellular DNA content to obtain a snapshot of the population of the cells in the cell cycle stages. The cell cycle stages were assigned in the histogram using markers in the FlowJo software (A). The percentage of H6 cell population in different cell cycle stages: sub-G₁ (B), G₀-G₁ (C), S (D), and G₂-M (E) are depicted. The mean \pm SD from three independent experiments is represented in the bars. The statistical analyses were performed using ordinary One-way ANOVA with Sidak's multiple comparisons test (B-H). (ns), (*), (**), (***), (****) indicate non-significant difference and the statistical differences of $p < 0.05$, $p < 0.01$, $p < 0.001$, and $p < 0.0001$ between the comparable indicated. Each datapoint is representative of independent experiment. Each independent experiment involved one biological replicate in 6-well plates.

Assessment of the effects of the lead compounds on activated mouse PMs

Primary mechanistic investigations in mouse cell lines showed that the leads are potent in suppressing IFN- γ -induced NO production. These observations led us to evaluate the leads in primary mouse macrophages *ex vivo*. Therefore, we sought to assess the effects of the leads on IFN- γ -activated PMs. Resident and Thioglycolate (TG)-elicited PMs were studied separately in the presence of the leads. TG-elicitation facilitates sterile inflammation in the peritoneal cavity, as it recruits small PMs at the site. These are physically, functionally, and developmentally distinct from the large resident PMs (Ghosn et al., 2010; Zaidi 2019). Studying both PM types helped to understand the effects of leads in different macrophage subsets. Among the leads tested, only auranofin significantly reduced the IFN- γ -induced nitrite production from both PM types (Fig.12A, D). The inhibitory response was concentration-dependent without cytotoxicity at a non-toxic concentration of 0.5 μ M (Fig.13). IFN- γ activation did not induce TNF- α production in the TG-elicited PMs. However, pentamidine, azithromycin, and auranofin significantly reduced the IFN- γ -induced IL6 production from TG-elicited PMs (Fig.12E, F).

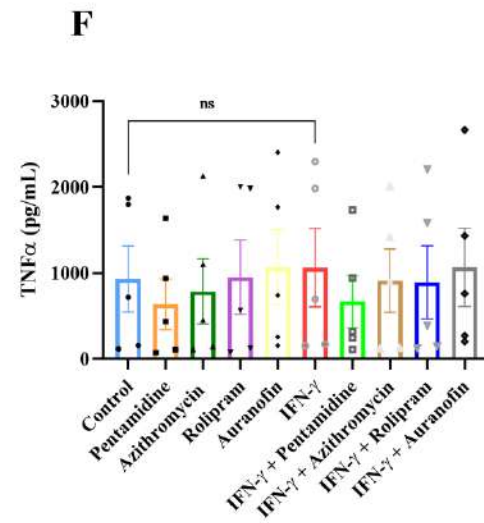
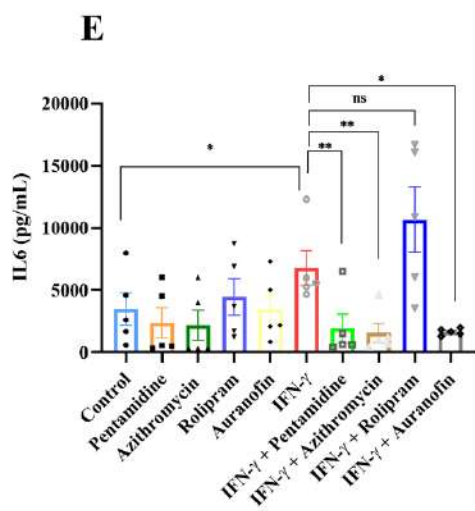
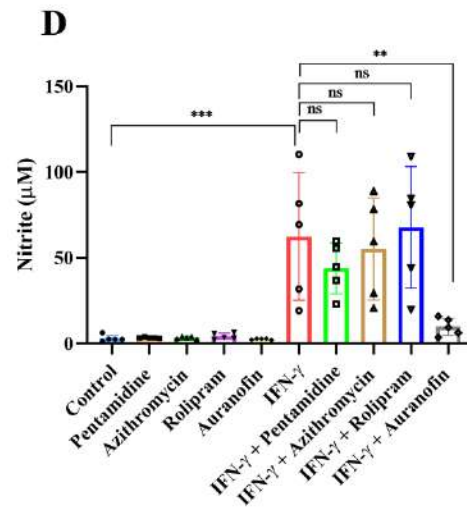
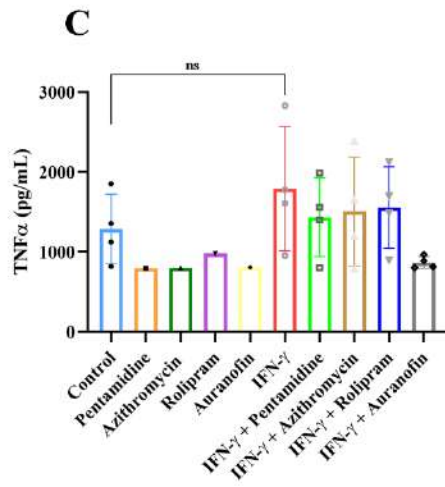
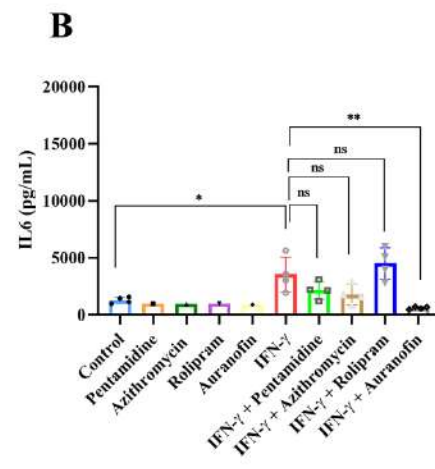
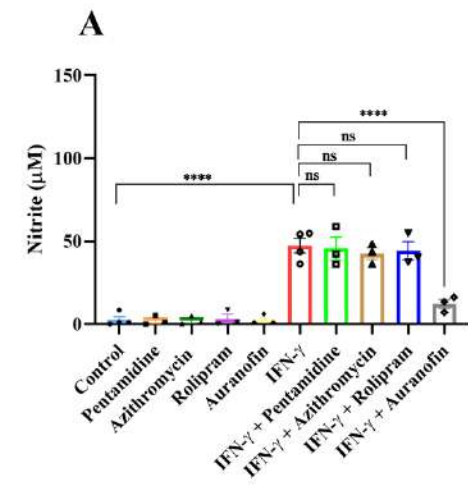


Fig.12. Auranofin lowers IFN- γ -induced nitrite and IL6 production in resident and TG-elicited primary mouse PMs.

Peritoneal macrophages were harvested from the peritoneal cavity of C57BL/6 mice and 2×10^5 cells were plated in each well of a 96-well plate. The cells were co-treated with 10 U/mL of IFN- γ and the lead compounds at the indicated concentrations. The cell-free supernatant was assayed after 24 hours for nitrite(A), IL6 (B) and TNF- α (C). TG-elicited macrophages were harvested from the peritoneal cavity of C57BL/6 mice after 4 days of intraperitoneal TG-injection. 2×10^5 cells were plated in each well of 96-well plate for the experimentation. The macrophages were co-treated with IFN- γ and the lead compounds. The cell-free supernatant was assayed after 24 hours for nitrite(D), IL6 (E) and TNF- α (F). The lead compounds were used at the following concentrations: pentamidine (1 μ M), azithromycin (40 μ M), rolipram (10 μ M), and auranofin (0.5 μ M). The statistical analyses were performed using ordinary One-way ANOVA with Sidak's multiple comparisons test (B-H). (ns), (*), (**), (***), (****) indicate non-significant difference and the statistical differences of $p < 0.05$, $p < 0.01$, $p < 0.001$, and $p < 0.0001$ between the comparable indicated. Each datapoint is representative of independent experiment. Data is represented as mean \pm SD of 3 to 5 independent experiments, each datapoint in the graph representing data from one mouse.

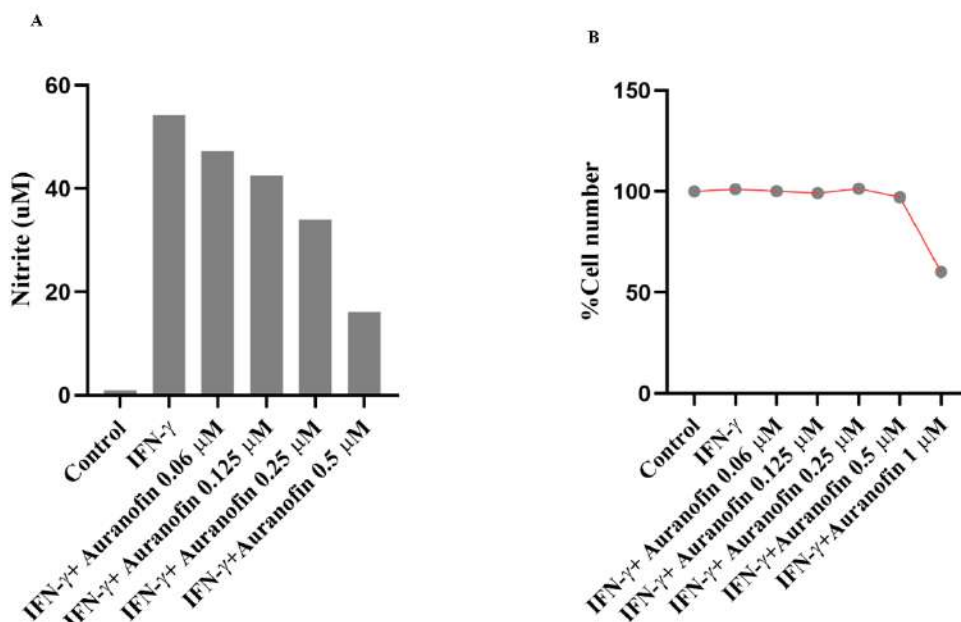


Fig.13. Auranofin reduces IFN- γ -induced nitrite formation in concentration dependent manner in TG-elicited PMs.

The concentration-dependent response of auranofin on nitrite production (A) and percent cell number change (B) by TG-elicited PMs to IFN- γ -stimulation. All the assays were performed after 24 hours of treatment as indicated. The statistical analyses were performed using ordinary One-way ANOVA with Sidak's multiple comparisons test. (ns), (*), (**), (***), (****) indicate non-significant difference and the statistical differences of $p < 0.05$, $p < 0.01$, $p < 0.001$, and $p < 0.0001$ between the comparable indicated. Each datapoint is representative of one independent experiment. Each independent experiment involved a pair of biological replicates in 96-well plates. The measurements were recorded in technical duplicates.

Evaluation of the four leads in an *in vivo* model of colitis in mice

The orthogonal assays in H6 cell lines and *ex vivo* tests on PMs indicated that these lead compounds may display anti-inflammatory effects. Dextran Sodium Sulfate (DSS) and 2,4,6-Trinitrobenzene sulfonic acid (TNBS)-induced colitis are widely used as *in vivo* mouse ulcerative colitis models. TNBS-induced colitis primarily depends on the Th1 response and CD4⁺ T cells (Antoniou et al., 2016). In contrast, DSS-induced colitis depends on CD4⁺ T cells, macrophages, and neutrophils, where IFN- γ signaling plays a vital role in disease pathogenesis (Shintani et al., 1998; Jones et al., 2018; Pathak et al., 2021). Therefore, we tested the usefulness of the identified lead compounds in DSS-induced ulcerative colitis. Initially, we tested the role of NOS2 in the disease pathogenesis of DSS-induced colitis. *Nos2*^{-/-} mice were compared against the wild-type counterparts in the progression of colitis and the outcome. Assessments with respect to colon length and DAI presented significant beneficial effects in the absence of the *Nos2* gene (Table 12, Fig.14). *Nos2*^{-/-} mice proved to be significantly resistant in the development of colitis, indicating that the presence and expression of the NOS2 play pivotal detrimental roles in colitis pathogenesis. This observation also suggested that inhibitors of IFN- γ -signaling-induced NOS2 activity could be advantageous as anti-inflammatory molecules against colitis.

Next, we tested the lead compounds in the mouse model of colitis. The compounds were injected intraperitoneally at 10 mg/kg bodyweight on days 2 and 4 of the commencement of oral DSS treatment. The mice were compared to wild-type mice, intraperitoneally injected with an equal dosage of DMSO as vehicle control. The treatment of azithromycin failed to improve the percent change in body weight. Although it could slightly improve the colon length but was not significant

due to variability. Rolipram showed a significant effect but displayed high variability. Pentamidine and auranofin proved to be significantly more beneficial than rolipram in rescuing the percent change in mouse body weight. A similar trend with statistical significance is reflected in the comparison of DAI (Table 13). Pentamidine and auranofin could significantly recover the DSS-induced reduction in colon length and improve DAI. On the other hand, the development of ulcerative colitis did not elevate serum TNF- α , but significantly increased IL6. Pentamidine, rolipram and auranofin reduced serum IL6, however, the effect of pentamidine was statistically significant (Fig.15). The overall *in vivo* assessment showed that pentamidine and auranofin have much better *in vivo* anti-inflammatory activities than others in colitis.

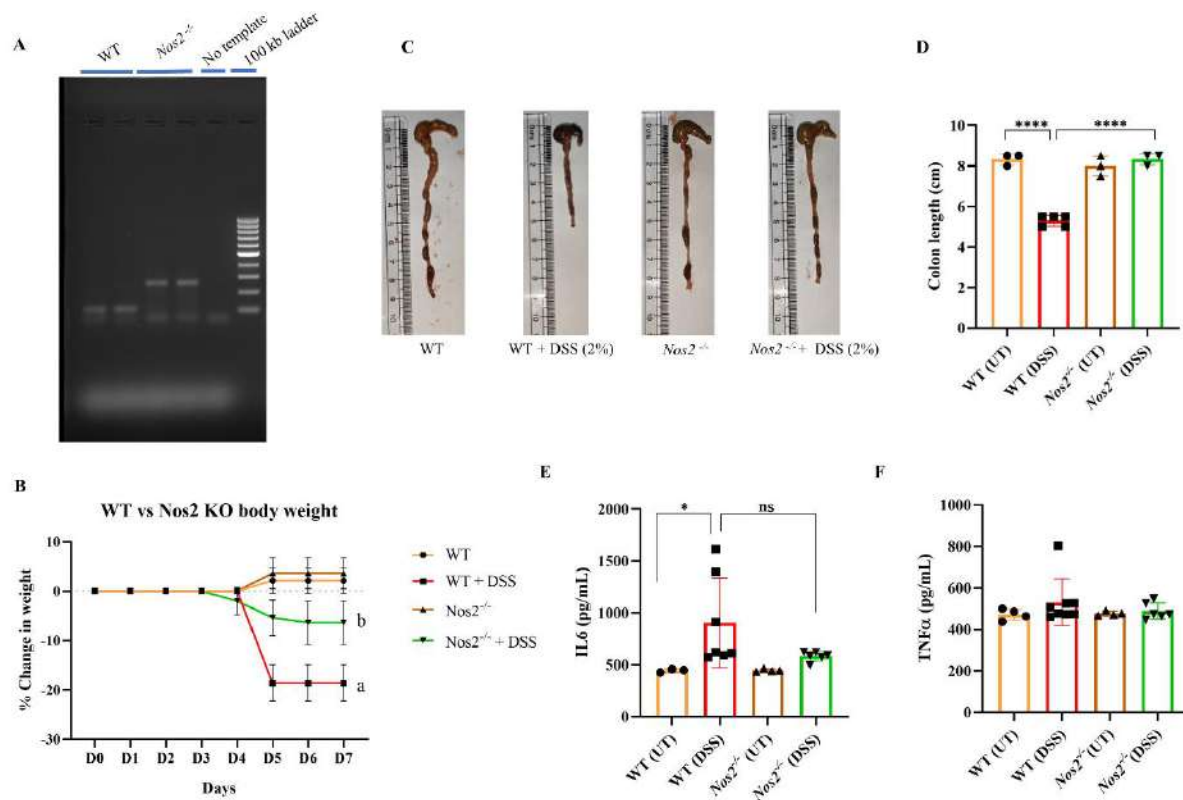


Fig.14. $Nos2^{-/-}$ mice are more protected from DSS-induced colitis than C57BL/6 WT mice.

Wild-type and $Nos2^{-/-}$ mice were challenged with DSS-induced colitis. The PCR-based confirmation of mouse genotype (A). C57BL/6 WT and $Nos2^{-/-}$ generate amplicon at 108 and 275 bp respectively. The change in percent

body weight (B) across 7 days of DSS treatment. Photographs of the colon from cecum to rectum (C) and the bar diagram of the pooled data of colon length (D). The serum level of IL6 (E) and TNF- α (F) after 7 days of DSS treatment. The statistical analyses were performed using mixed effect two-way ANOVA with Tukey's multiple comparisons test (B) and ordinary One-way ANOVA with Sidak's multiple comparisons test (D, E, F). (a) and (b) indicate (WT vs. WT + DSS, $p < 0.01$) and (WT + DSS vs. *Nos2*^{-/-} + DSS, $p < 0.01$) on day 7, respectively (B). (ns), (*), (**), (***) (****) indicate non-significant differences, and the statistical differences of $p < 0.05$, $p < 0.01$, $p < 0.001$, and $p < 0.0001$ between the comparable indicated (D, E, F). Each data point is representative of mean + SD from 3-7 mice (B) or represents a mouse and cumulatively is depicted as mean + SD (D, E, F).

Table 12. DAI scores between C57BL/6 and *Nos2*^{-/-}

Disease activity index (DAI score) are composed of the change of body weight, diarrhea, and hematochezia. Statistical analysis was performed using two-way ANOVA with Tukey's multiple comparison test. Data are presented as means \pm SDs. a, $p < 0.01$ (WT vs. WT+DSS); b, $p < 0.05$ (WT+DSS vs *Nos2*^{-/-} + DSS). D, day of administration; DSS, dextran sodium sulfate.

	D0	D1	D2	D3	D4	D5	D6	D7
WT	0	0	0	0	0	0	0	0
WT+DSS	0	0	0	0	1 \pm 1.67	4 \pm 1.09	7.5 \pm 2.58	11 \pm 1.54 (a)
<i>Nos2</i> ^{-/-}	0	0	0	0	0	0	0	0
<i>Nos2</i> ^{-/-} + DSS	0	0	0	0	0.5 \pm 0.54	0.83 \pm 0.4	1.33 \pm 1.36	3.66 \pm 2.87 (b)

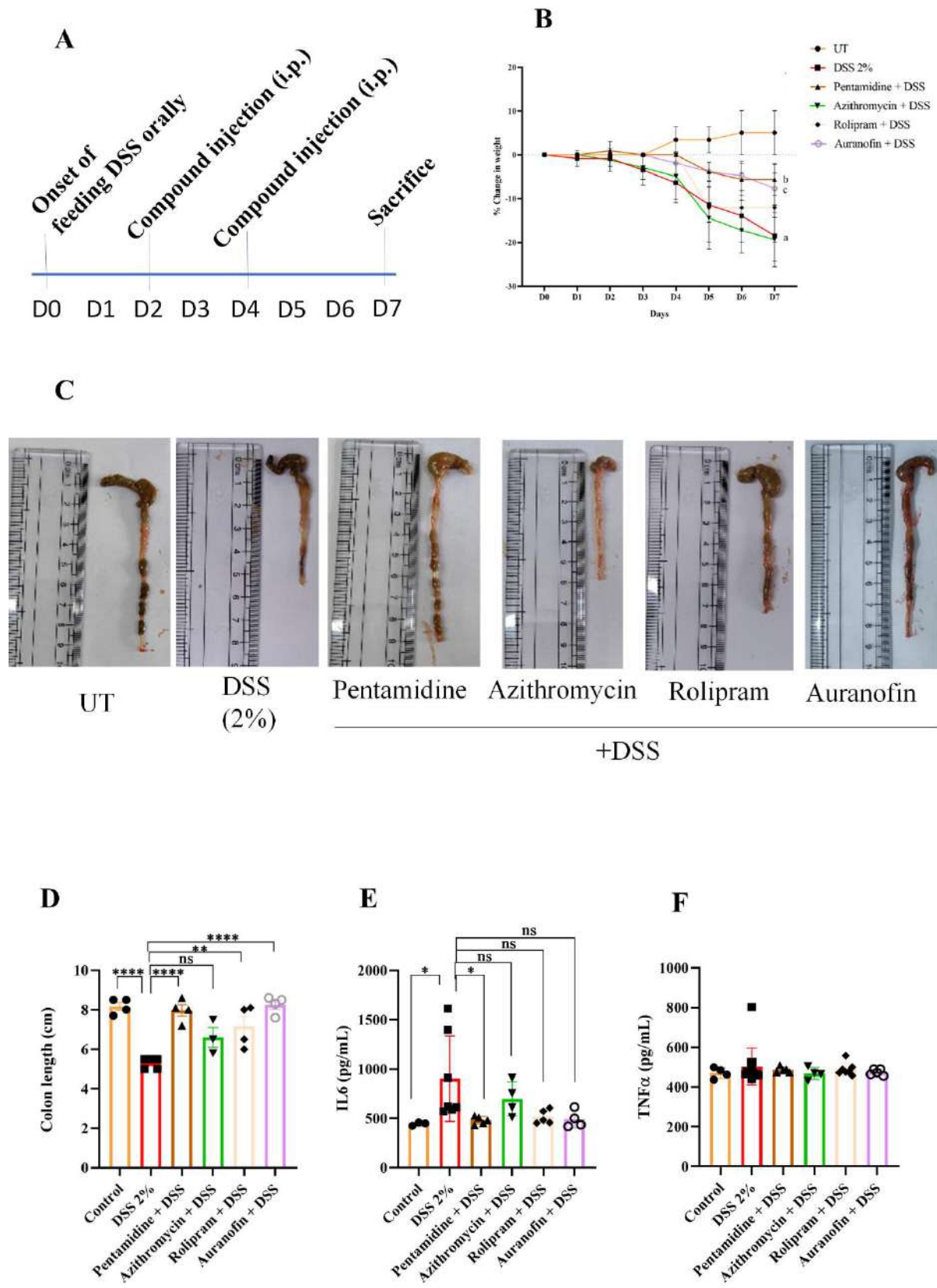


Fig.15. Pentamidine and auranofin display the most potent anti-inflammatory effects in an *in vivo* model of DSS-induced mouse colitis.

Wild-type C57BL/6 mice were challenged with DSS-induced colitis. The treatment timeline of DSS and lead compounds is depicted (A). Change in percent body weight across 7 days of DSS treatment (B). Photographs of the colon from cecum to rectum (C) and the bar diagram of the pooled data of colon length (D). The serum level of IL6 (E) and TNF- α (F) after 7 days of DSS treatment. The statistical analyses were performed using two-way ANOVA with Tukey's multiple comparisons test (B) and ordinary One-way ANOVA with Sidak's multiple comparisons test (D, E, F). (a), (b) and (c) indicate (UT vs. DSS, $p < 0.001$), (DSS vs. Pentamidine + DSS, $p < 0.001$), and (DSS vs. Auranofin + DSS, $p < 0.001$) on day 7, respectively (B). (ns), (*), (**), (***), (****) indicate non-significant differences, and the statistical differences of $p < 0.05$, $p < 0.01$, $p < 0.001$, and $p < 0.0001$ between the comparable indicated (D, E, F). Each data point is representative of mean \pm SD from 6-7 mice (B) or represents a mouse and cumulatively is depicted as mean \pm SD (D, E, F).

Table 13. DAI scores of the lead compounds in DSS-induced colitis

Disease activity index (DAI score) are composed of the change of body weight, diarrhea, and hematochezia.

Statistical analysis was performed using two-way ANOVA with Tukey's multiple comparison test. Data are

presented as means \pm SDs. a, $p < 0.01$ (UT vs. DSS); b, $p < 0.01$ (DSS vs Pentamidine isethionate + DSS); $p < 0.05$

(DSS vs Auranofin + DSS). D, day of administration; UT, Untreated; DSS, dextran sodium sulfate.

	D0	D1	D2	D3	D4	D5	D6	D7
UT	0	0	0	0	0	0	0	0
DSS treatment	0	0.16 \pm 0.4	0.16 \pm 0.4	0.5 \pm 0.54	2.33 \pm 1.5	4.66 \pm 1.86	6.33 \pm 2.87	11 \pm 1.54 (a)
Pentamidine isethionate + DSS	0	0	0	0	0	0.66 \pm 0.51	1.33 \pm 1.36	3.16 \pm 2.22 (b)
Azithromycin dihydrate + DSS	0	0	0.16 \pm 0.4	0.5 \pm 0.54	2 \pm 1.09	4.5 \pm 2.88	8.66 \pm 4.45	10 \pm 3.03
Rolipram + DSS	0	0	0	0	0	2.66 \pm 2.33	4.83 \pm 3.12	7.16 \pm 1.83
Auranofin + DSS	0	0	0	0	0.5 \pm 0.54	0.83 \pm 0.4	3.16 \pm 2.04	4.83 \pm 2.48 (c)

Pentamidine and Auranofin improve survival of mice during sepsis

It was important to address whether these two compounds were effective in another inflammatory disease mice model. Therefore, we induced peritonitis sepsis by intraperitoneal injection of *Salmonella* Typhimurium in mice (Yadav et al., 2018; Chattopadhyay et al., 2022). To mimic the clinical scenario, the compounds were intraperitoneally injected after 3-4 hr post injecting the bacteria. Pentamidine proved to be significantly effective at 10 mg/kg body weight dose in improving the survival of mice in sepsis. Auranofin greatly enhanced survival at 0.3 and 1 mg/kg body weight doses. The Kaplan-Meier survival analysis demonstrated that the median survival of pentamidine at 10 mg/kg body weight and auranofin at 0.3 mg/kg body weight treatment improved to 60 and 66 hours, respectively, in comparison to untreated septic mice, which were 24 hours (Fig. 3.15). The log-rank test for trend showed a p-value of <0.0001, indicating statistical significance for the survival of compound-treated mice.

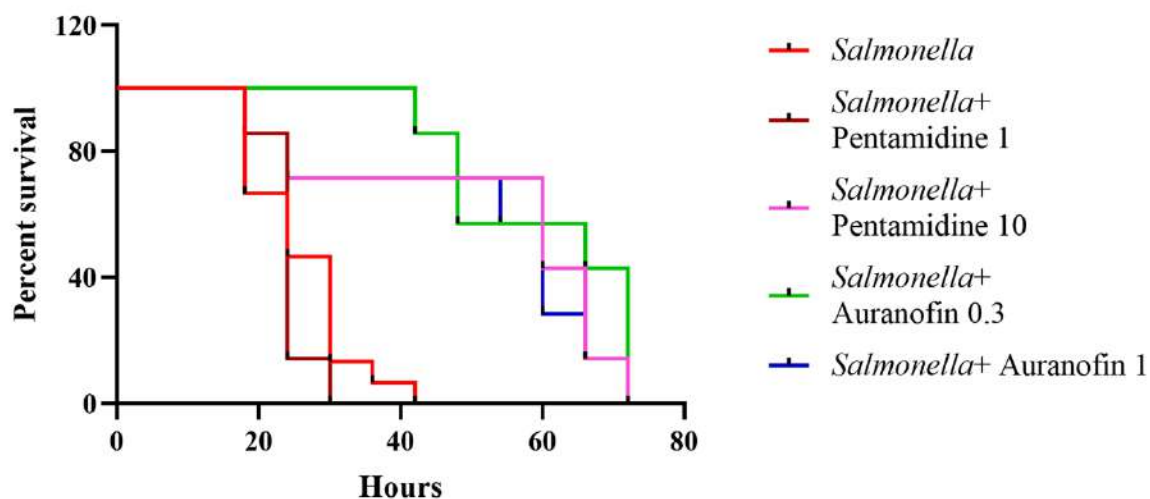


Fig.16. Pentamidine and auranofin improve survival in peritonitis sepsis in mice.

BALB/c mice were intraperitoneally injected with *Salmonella* Typhimurium to induce sepsis. Pentamidine and auranofin were intraperitoneally administered 3 hours post infection. The numbers after compound names indicate the dosage in mg/kg body weight of mice. Each condition comprised of 6-9 mice of 6-8 weeks old and 22-24g of body weight. The survival data is demonstrated as Kaplan-Meier plot.

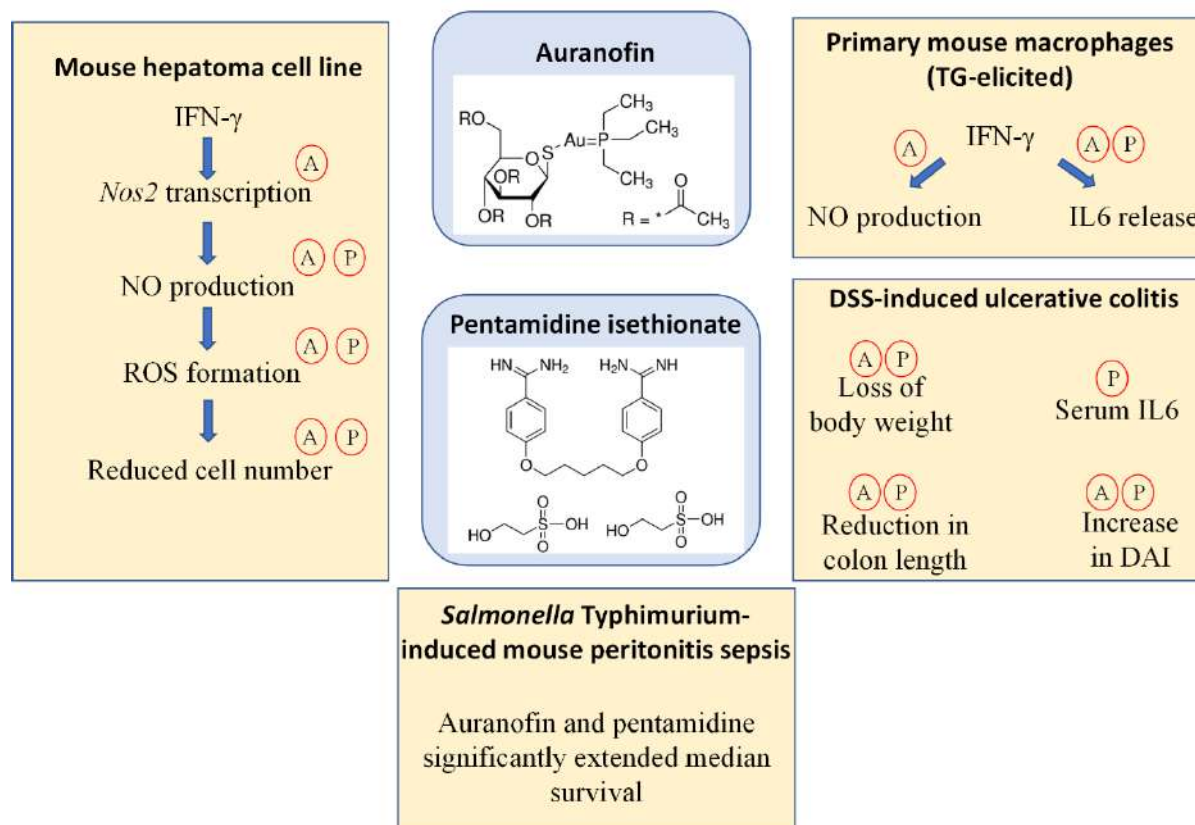


Fig.17. A model depicting the role of auranofin and pentamidine as anti-inflammatory compounds in *in vitro* and *in vivo* settings.

The figure depicts the summary of the inhibitory effects of the top two lead compounds: auranofin and pentamidine. The chemical structures of the lead compounds are depicted in the middle. In this figure, 'A' and 'P' indicate the inhibitory effect of auranofin and pentamidine respectively in the cellular and biological processes mentioned. The effects are categorized in mouse hepatoma cell line H6, TG-elicited primary mouse macrophages and DSS-induced mouse ulcerative colitis. Auranofin significantly reduced the IFN- γ -induced nitrite production by reducing transcription of *Nos2*, whereas pentamidine presumably affected at the post-transcriptional level to reduce nitrite. All these culminated into the reduction of intracellular ROS and increased cell survival in the presence of IFN- γ . Pentamidine reduced the IFN- γ -induced IL6 production from TG-elicited primary mouse macrophages, whereas auranofin potently reduced IFN- γ -

activated nitrite and IL6 production. Importantly, auranofin and pentamidine demonstrated protective effects in DSS-induced mouse ulcerative colitis *in vivo*. Also, auranofin and pentamidine significantly extended the survival of mice during *Salmonella* Typhimurium-induced sepsis.

Assessment of the combinatorial effects of pentamidine and auranofin in sepsis and colitis

Pentamidine proved to be significantly effective at 10 mg/kg body weight dose in improving the survival of mice in sepsis. Auranofin greatly enhanced survival at 0.3 and 1 mg/kg body weight doses (Fig.16). We asked whether combining these two compounds can exhibit any additive or synergistic effect in sepsis. Therefore, pentamidine and auranofin were intraperitoneally administered in combination at different doses. The combination of pentamidine 1 and auranofin 0.3 mg/kg body weight did not improve the survival of septic mice. The mixtures of compounds did not exhibit any synergistic effect. However, the combination of pentamidine 10 and auranofin 1 mg/kg body weight showed similar improvement in survival compared to compound-alone controls. Therefore, the compounds did not antagonize in improving the survival of septic mice (Fig.18)

Next, we addressed whether the combinations of pentamidine and auranofin can improve disease pathogenesis in ulcerative colitis. A similar approach to the compound combination was undertaken with the combination of pentamidine and auranofin at lesser and higher doses. These dosages were kept much lower than 10 mg/kg body weight, which was used in the experiment of comparative analyses involving all four compounds (Fig.15). Although auranofin alone failed to show any effect at 1 mg/kg body weight, pentamidine alone slightly improved colitis disease pathogenesis at 3 mg/kg body weight. The combination of pentamidine 0.6 and auranofin 0.2 mg/kg body weight showed significant response variations. The combination of pentamidine 3 and auranofin 1 mg/kg body weight significantly improved the body weight of mice, disease activity index, and colon length. The latter combination of pentamidine and auranofin synergized in protecting the mice from the development of colitis (Fig.19, Table 14).

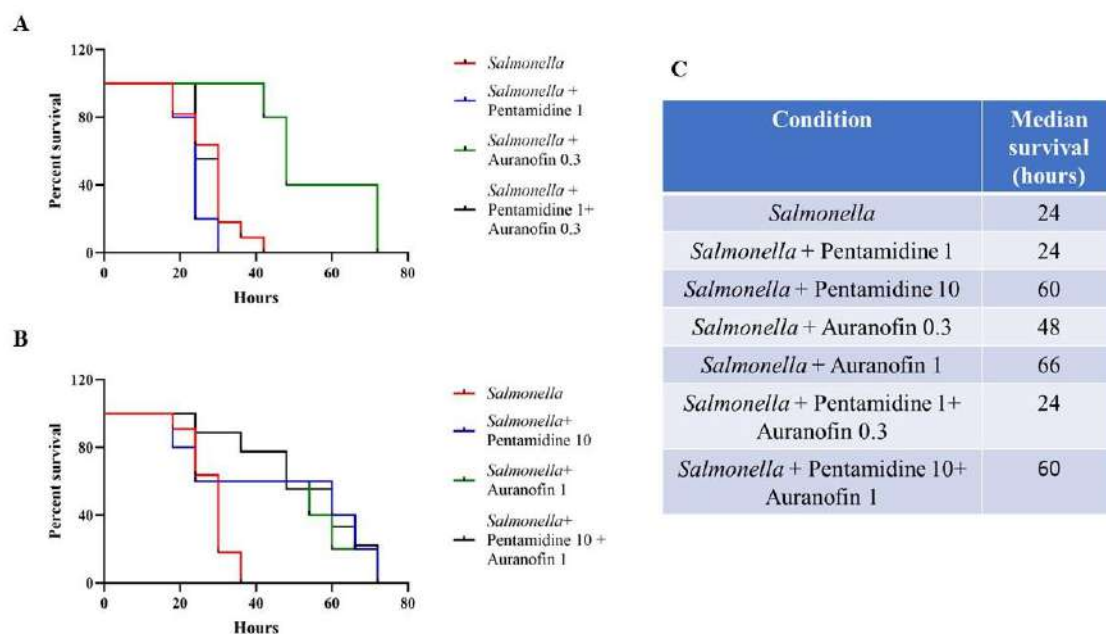


Fig.18. Pentamidine and auranofin in combination do not synergize in protection against sepsis

The figure demonstrates the survival profile of *Salmonella* typhimurium-induced sepsis in BALB/c mice. The mice were intraperitoneally injected with *Salmonella* Typhimurium to induce sepsis. Pentamidine and auranofin were intraperitoneally administered 3 hours post-infection. The numbers after compound names indicate the dosage in mg/kg body weight of mice. Figure A and B indicates the survival of mice upon treatment with the combination of pentamidine and auranofin at lesser and higher dosage, respectively. Each condition comprised 6-9 mice 6-8 weeks old and 22-24g of body weight. The survival data are demonstrated as a Kaplan-Meier plot. The median survival in hours of each condition is tabulated (C).

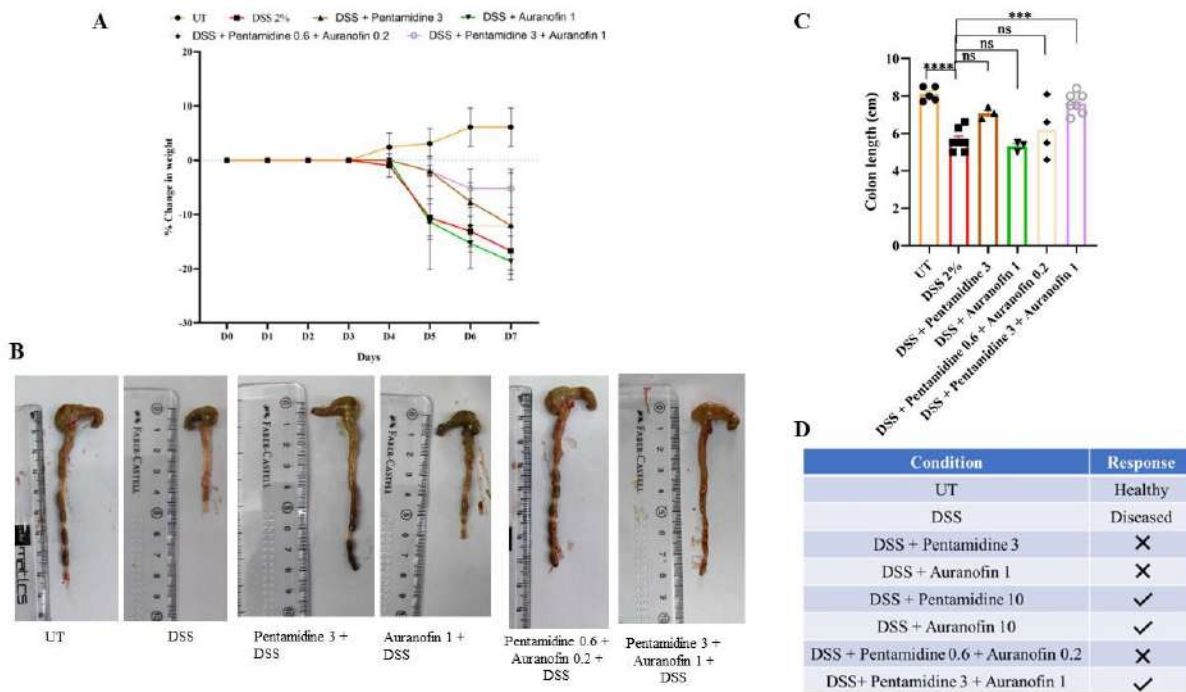


Fig.19. Pentamidine and auranofin synergize in DSS-induced ulcerative colitis in mice

The percent change in body weight is demonstrated on a timespan of 7 days, indicated on the x-axis as D, followed by the number of days (A). The colon images and bar diagram of colon length are shown here (B, C). Each data point indicates a mouse (C). The numbers after compound names indicate the dosage in mg/kg body weight of mice. The response in each condition is tabulated with (✗) indicating no rescue and (✓) indicating significant rescue. The statistical analyses were performed using ordinary One-way ANOVA with Sidak's multiple comparisons tests. (ns), (*), (**), (***), (****) indicate non-significant difference and the statistical differences of $p < 0.05$, $p < 0.01$, $p < 0.001$, and $p < 0.0001$ between the comparable indicated. Each data point is representative of mean + SD from 3-9 mice.

Table 14. DAI scores of the compound-combinations in DSS-induced colitis

The disease activity index (DAI score) is composed of changes in body weight, diarrhea, and hematochezia. The compounds were administered intraperitoneally on days 2 and 4 of the oral DSS treatment. The numbers after compound names indicate the dosage in mg/kg body weight of mice. Data are presented as means \pm SDs. a, $p < 0.01$ (UT vs. DSS); b, $p < 0.01$ (DSS vs medium combination + DSS). D, day of administration; UT, Untreated; DSS, dextran sodium sulfate; low combination, pentamidine 0.6 and auranofin 0.2 mg/kg body weight; medium combination, pentamidine 3 and auranofin 1 mg/kg body weight.

	D0	D1	D2	D3	D4	D5	D6	D7
UT	0	0	0	0	0	0	0	0
DSS	0	0	0	0	1.23 \pm 0.5	3.66 \pm 1.67	6.33 \pm 2.5	10.76 \pm 1.54 (a)
Pentamidine 3 + DSS	0	0	0	0	1 \pm 0.2	1.5 \pm 0.7	3.4 \pm 2.5	7.5 \pm 3.5
Auranofin 1 + DSS	0	0	0	0	1.25 \pm 0.8	3.57 \pm 1.8	7.45 \pm 3.4	10.9 \pm 2.7
Pentamidine 0.6 + Auranofin 0.2+ DSS	0	0	0	0	0	2.8 \pm 2.16	5.2 \pm 4.86	7.4 \pm 4.17
Pentamidine 3 + Auranofin 1+ DSS	0	0	0	0	0	0.33 \pm 0.5	1.33 \pm 1.36	2.33 \pm 1.5 (b)

Statistical analyses

All graphical representations and statistical analyses were performed on GraphPad Prism software version 8.0.2. All data are represented as mean \pm standard deviation of the mean (SD) unless stated otherwise. The data distribution was tested using QQ-plot to examine the skewness. Statistical analyses were performed using ordinary One-way ANOVA with Sidak's multiple comparisons tests and two-way ANOVA with Tukey's multiple comparisons tests. (ns), (*), (**), (***), (****)

indicate non-significant difference and the statistical differences of $p < 0.05$, $p < 0.01$, $p < 0.001$, and $p < 0.0001$, respectively, between the comparable indicated, unless stated otherwise.

Discussion

The high-throughput screening of the LOPAC^{®1280} targeting IFN- γ -induced NO production led to the identification of four novel pharmacological inhibitors of the inflammatory signaling process: pentamidine, azithromycin, rolipram, and auranofin. The primary targets of the lead compounds are as follows. Pentamidine is an NMDA receptor antagonist and used to treat *Pneumocystis* pneumonia, leishmaniasis, and trypanosomiasis (Salamone & Cunha, 1988). Also, pentamidine is reported to bind tRNA non-specifically and dampen translational processes (Sun & Zhang, 2008). Azithromycin binds to the 50S subunit of the 70S bacterial ribosome to block translation (Sultana et al., 2020). It is used against bacterial infections as an antibiotic and cystic fibrosis due to its anti-inflammatory properties (Principi et al., 2015). Rolipram inhibits phosphodiesterase 4 (PDE4) and elevates intracellular cyclic AMP (cAMP) (Huang et al., 2019). Auranofin, a gold(I) compound with phosphine and thiol ligands in a linear arrangement, primarily inhibits thioredoxin reductase (Zhang et al., 2019), which is critically involved in maintaining normal protein function and combating oxidative damage. Auranofin is typically used in combination with other medications, such as non-steroidal anti-inflammatory drugs (NSAIDs) or disease-modifying antirheumatic drugs (DMARDs), to help control the symptoms of rheumatoid arthritis (Roder & Thomson, 2015). However, the clinical use of auranofin against rheumatoid arthritis declined in the last decade. The decline may be due, in part, to the inclusion of more effective DMARDs, such as methotrexate (Doan & Massarotti, 2005). Nevertheless, auranofin presents an excellent potential for drug repurposing in various diseases. Notably, auranofin inhibits SARS-CoV-2 replication, ACE-2-dependent SARS-CoV-2 endocytosis and inhibits PLpro, the papain-like protease of SARS-CoV-2 (Gil-Moles et al., 2020). In addition, auranofin's anti-inflammatory properties protect against neurodegenerative disorders, such as Alzheimer's and Parkinson's disease (Gil-Moles et al., 2020). Three out of four leads, namely, auranofin (trade name: Ridaura), pentamidine (trade name: Pentam 300), and azithromycin (trade name: Zithromax), are FDA-approved

marketed drugs. Rolipram is not FDA-approved because clinical trials of the drug have not consistently shown positive results. Alternatively, roflumilast (trade name: Daliresp) has the same activity as rolipram and is FDA-approved marketed drug.

A systematic evaluation of the leads in cell lines, primary mouse macrophages, and *in vivo* mouse disease model ranked auranofin as the top-active lead. This conclusion is comparatively drawn from the best goodness of fit on IFN- γ -induced NO production *in vitro*, the most effective transcriptional repression of IFN- γ -induced *Nos2* expression, the only compound to abolish NO production in activated primary macrophages, and the significant beneficial effect in DSS-induced mouse colitis. Based on *in vivo* experiments, pentamidine and auranofin emerged as the most potent compounds from the LOPAC^{®1280} library which can be repurposed for use in inflammatory diseases. A summary of the inhibitory effects of auranofin and pentamidine is depicted in Fig. 3.16. To understand the mechanisms by which these compounds may be affecting the IFN γ -induced NO pathway, further *in silico* studies were performed. SWISSTargetPrediction showed that pentamidine has a probability score of 1 for targeting proteases and family A G-protein coupled receptors. It may target 33.3% of family A G-protein coupled receptors (Fig.20A). Molinspiration showed that pentamidine possesses a bioactivity score of 0.6 as a protease inhibitor and 0.35 as GPCR ligand (Fig.S8B). The IFN- γ -activated signaling pathway is less likely to be influenced by proteases unless the proteases proteolytically activate proteins assisting NOS2 function. It is more likely to be affected by the GPCR signaling pathway at the suboptimal concentration used in this study. Therefore, pentamidine's non-canonical modulation of the GPCR pathway may cause signaling crosstalk and underlie the reduction of nitrosative and oxidative effects of IFN- γ (Fig.21). SWISSTargetPrediction also showed that auranofin may target 46.7% of kinases. Molinspiration showed that auranofin is predicted to have only enzyme inhibitor activity with a bioactivity score of 0.31 (Fig.20 C, D). The IFN- γ signaling pathway largely depends on the phosphorylation cascade for transcriptional activation. For instance, the phosphorylation of transcription factors like IRF1 and NF- κ B is essential for the IFN- γ -activated transcription of *Nos2*. Auranofin may inhibit some kinase functions to downregulate the *Nos2* transcription upon IFN- γ signaling (Fig.21).

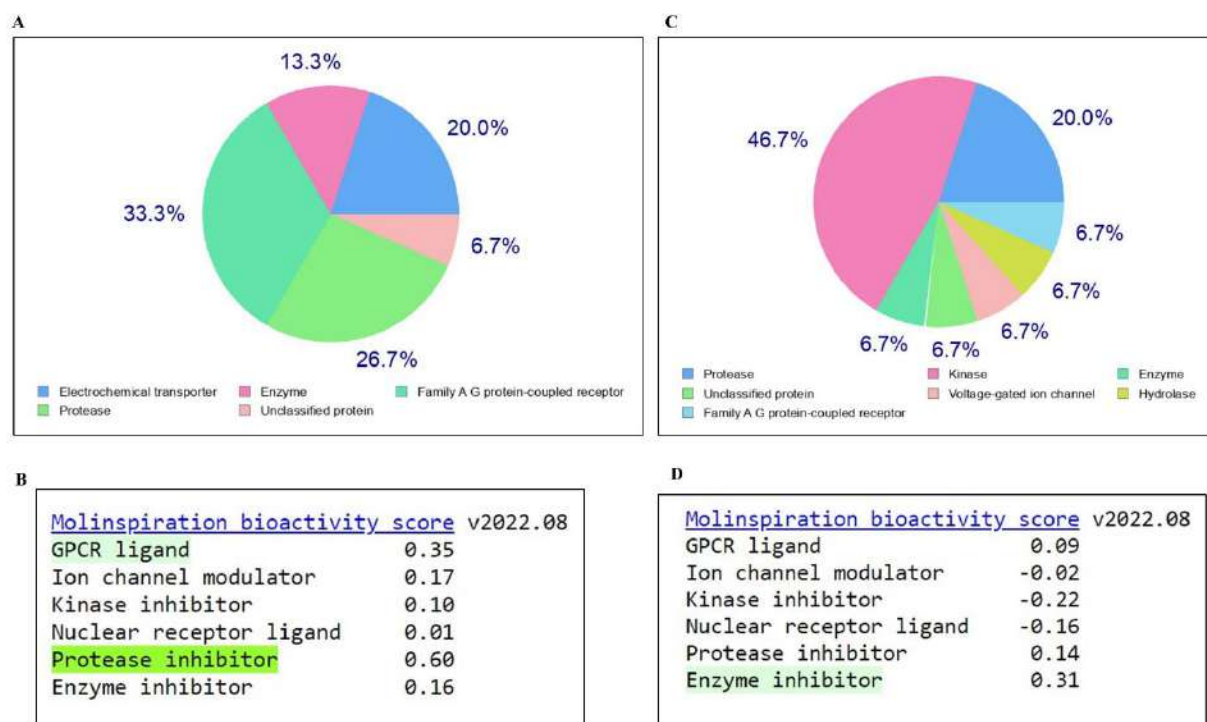


Fig.20. Pentamidine may inhibit proteases and/or modulate GPCR signaling, whereas auranofin may target kinase function.

SWISSTargetPrediction and Molinspiration-based analysis of compound target prediction and bioactivity for pentamidine (A, B) and auranofin (C, D).

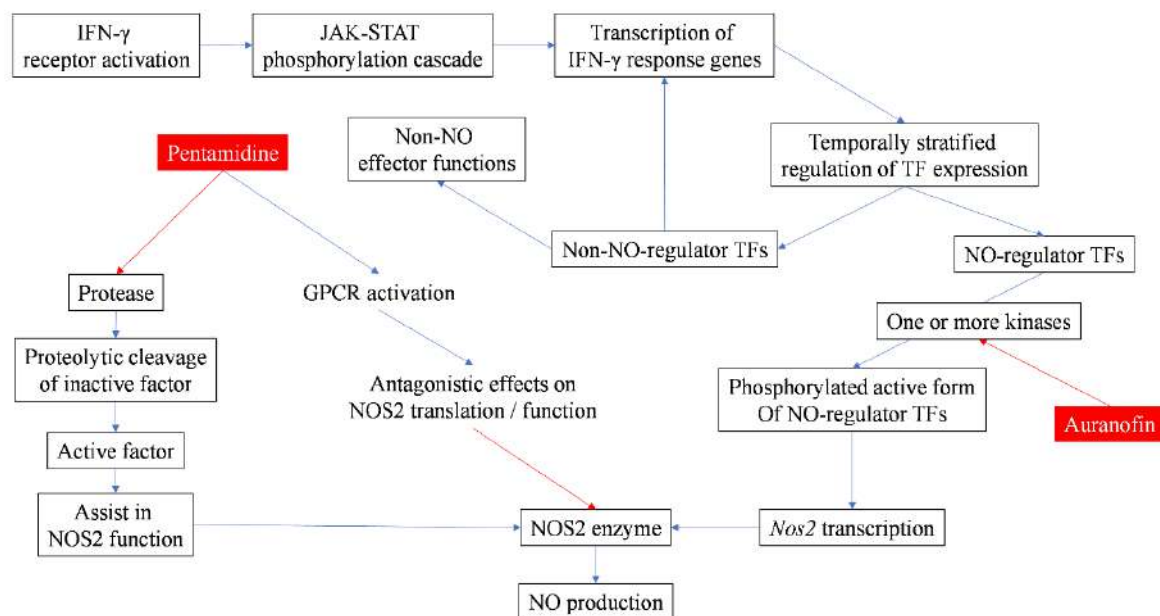


Fig.21. A hypothetical model depicting the mechanistic targets of pentamidine and auranofin in the IFN- γ -NO pathway

A graphical representation of the hypothetical model based on cheminformatics prediction analysis and experimental evidence obtained from this study is demonstrated here. IFN- γ activation leads to the JAK-STAT phosphorylation cascade as canonical signaling pathway. Pentamidine may either target proteases involved in proteolytic cleavage and activation of proteins assisting NOS2 function, or may activate GPCR pathway to antagonize the NO-dependent arm of IFN- γ signaling. Auranofin may inhibit one or more kinases involved in the phosphorylation of transcription factors, essential in *Nos2* transcription. The nodes with black outline represent the components of IFN- γ signaling pathway. Red filled boxes show the position of pentamidine and auranofin in the map. The blue and red arrows indicate activation and inhibition, respectively. TF: Transcription factor, GPCR: G protein coupled receptor, NO: Nitric Oxide, NOS2: Nitric oxide synthase 2, JAK: Janus kinase, STAT: Signal transducer and activator of transcription.

IFN- γ often imparts immunomodulatory and anti-tumor effects by regulating cell proliferation and survival. Several studies deciphered the mechanism of action in inflammatory conditions and malignancy (Kotredes & Gamero, 2013; Lee et al., 2017). For instance, in vitiligo, IFN- γ promotes the expression of pro-apoptotic factors Bax, Bak, and cleaved caspase-3 in melanocytes to induce apoptosis (Su et al., 2020). IFN- γ plays a crucial role in pushing Toll-like receptor-activated microglia towards neurotoxic states that lead to the emergence of energetic and oxidative stress, significant impairment in network functioning, and, ultimately, neuronal demise (Kann et al., 2022). IFN- γ has dual effects in the tumor microenvironment, from tumor elimination to escape. Consequently, the interaction between IFN- γ and the immune system within the tumor determines the outcome of the tumor in a person with cancer (Alspach et al., 2019). Studies using several mouse tumor cell lines demonstrated that some tumor types are more selectively susceptible to IFN- γ -mediated cell cycle arrest and apoptosis. A mechanistic investigation on IFN- γ -mediated tumor apoptosis revealed that the cell proliferation blockade and apoptosis in H6 hepatoma and L929 fibrosarcoma mouse cell lines depend on IFN- γ -induced NOS2-mediated NO production. NO elevates intracellular peroxynitrite and ROS and activates the Jnk pathway, culminating in cell death (Prasanna et al., 2007; Rakshit et al., 2014). The IFN- γ -activation also reduces cell number in the Renca renal adenocarcinoma cell line (Gao et al., 2016; Su et al., 2020). This study demonstrates that all four leads effectively reduced IFN- γ -induced NO production in at least two of three cell lines H6, RAW 264.7, and Renca. Pentamidine inhibited IFN- γ -mediated NO production and rescued cell numbers in all three cell lines to different extents, indicating that its effects are not cell-line restricted. Although auranofin effectively retarded the NO production in these cell lines, it rescued IFN- γ -mediated cell number reduction only in H6. The underlying reason might be the extent of the reduction in NO production. Auranofin moderately reduced NO production in RAW 264.7 and Renca but entirely in H6. Auranofin most effectively released the IFN- γ -activated H6 cells from the arrest at S-phase. These support the notion that the regulation and outcome of the IFN- γ -signaling pathway varies between cell types. A detailed mechanism of action study needs to be performed to understand the effects of the compounds on apoptosis.

The IFN- γ activation leads to the promoter occupancy of *Nos2* by STAT1, IRF1, and Interferon stimulated gamma factor (ISGF) 3 complex (comprising STAT1, STAT2, and IRF9), leading to the expression of *Nos2* mRNA. Other transcription factors (such as NF- κ B and HIF1 α) can also bind the promoter of *Nos2*, synergistically enhancing its transcription (Kleinert et al., 2010; Bogdan,

2015). Therefore, the regulation of *Nos2* expression is governed by several transcription factors, and the mode of regulation can be context dependent. In this study, only pentamidine and azithromycin reduced the expression of *Irf1*, one of the transcription factors regulating *Nos2* expression. All the lead compounds reduced *Nos2* expression, where the effect of azithromycin, rolipram, and auranofin was significant. On the other hand, IFN- γ activates the cyclic adenosine monophosphate (cAMP)-pathway, which regulates IFN- γ signaling in PMs (Liu et al., 2004). The present study demonstrates that rolipram, a cAMP-elevating agent, further upregulates the NO-independent arms of IFN- γ signaling: *Tap2* and *Cd274*. Whether the IFN- γ and cAMP signaling processes synergize at the NO-independent arms remains to be explored. In addition, none of the four leads affected IFN- γ -induced elevation of the MHC Class 1 surface expression in H6 cells, suggesting that the NO-independent processes of the IFN- γ -signaling armamentarium might remain unaffected. Thus, the leads are unlikely to impair the antigen presentation processes and possess broad off-target signal diminution effects. On the other hand, all the leads significantly reduced IFN- γ -induced intracellular accumulation of ROS in H6 cells. Our observations indicate that the leads can protect IFN- γ -stimulated cells from oxidative damage without hampering the endogenous antigen processing and presentation pathway.

Previous studies showed that auranofin inhibits NO production in LPS-stimulated RAW 264.7 macrophages. However, it remained unclear whether auranofin can reduce IFN- γ -induced NO production (Han et al., 2008). Herein, we demonstrate that auranofin effectively inhibited IFN- γ -induced NO production and scored the best goodness of fit in the nonlinear regression analysis of IC₅₀ among the hits compared. Auranofin also lowered intracellular ROS in the IFN- γ -activated H6 cells. Although existing literature suggests that auranofin increases intracellular ROS by impairing cellular antioxidant machinery in unstimulated cells (Zou et al., 2015), it reduced IFN- γ -mediated enhancement of oxidative stress in IFN- γ -activated H6 cells. Rakshit et al demonstrated that IFN- γ -induced NO production is primarily responsible for the increased ROS in the H6 cells (Rakshit et al., 2014). Therefore, the auranofin-mediated interference of IFN- γ -induced *Nos2* expression and subsequent reduction of NO production can be attributed to the reduction in IFN- γ -induced oxidative stress.

IFN- γ -activation-induced M1 polarization of macrophages, and excessive NO production is implicated in several inflammatory diseases, including acute peritonitis and peritonitis sepsis. The

activation facilitates the production of several pro-inflammatory cytokines and chemokines. In addition, when mice are exposed to a lethal dosage of LPS, antibody-mediated inhibition of IFN- γ reduces systemic inflammation and increases survival (Romero et al., 2010). Herein, we report that auranofin potently reduced IFN- γ -induced NO and IL6 production. Previous reports revealed that auranofin reduces the dimerization of LPS-receptor Toll-like receptor 4 and impairs NF- κ B activation in RAW 264.7 macrophage cell line (Youn et al., 2006; Hwangbo et al., 2021). However, the contribution of NF- κ B in IFN- γ -inducible *NOS2* expression and NO production is minimal in macrophages, whereas the IFN- γ -dependent STAT1 α plays an essential role. Erk1/Erk2 contributes to the full activation of STAT1 α by mediating STAT1 α Ser727 residue phosphorylation in IFN- γ -stimulated macrophages (Romero et al., 2010). Whether auranofin can interfere with these kinase functions remains to be investigated. Similar investigations are also required with pentamidine and azithromycin on suppressing IFN- γ -mediated IL6 production.

Inflammatory bowel disease (IBD) refers to two conditions, Crohn's disease, and ulcerative colitis. Both conditions involve chronic digestive tract inflammation, but they affect different parts of the digestive system. Crohn's disease can affect any part of the digestive tract, from the mouth to the anus. In contrast, ulcerative colitis is usually only in the innermost lining of the large intestine (colon) and rectum (Romero et al., 2010). The persistence of ulcerative colitis increases the risk of developing colorectal carcinoma (Lakatos & Lakatos, 2008). A study in IBD patients demonstrated that IFN- γ -induced NO pathway plays a pivotal role in ulcerative colitis pathogenesis (Rafa et al., 2010a). Therefore, we expanded the lead evaluation process from *in vitro* tumor cell line and *ex vivo* PMs to *in vivo* disease model of ulcerative colitis to test their efficacy in the body. DSS-mediated experimental ulcerative colitis pathogenesis in mice strongly depends on the elevation of IFN- γ in intestinal tissue and IFN- γ -triggered inflammatory processes (Ito et al., 2006; Langer et al., 2019). Here we demonstrate that *Nos2*^{-/-} mice are protected from DSS-mediated ulcerative colitis in mice. This observation suggests that IFN- γ -induced NOS2 activation might be involved in colitis pathogenesis. Thus, we evaluated the leads in DSS-induced ulcerative colitis in mice. The anti-protozoal drug pentamidine is already reported to ameliorate DSS-induced mouse colitis, likely targeting S100B activity (Esposito et al., 2012). However, the plan of drug administration was dissimilar. In this comparative study among lead compounds, azithromycin failed to show any significant beneficial effect. This macrolide antibiotic might mechanistically target tumor-specific NO production processes but not in primary cells or *in vivo* disease conditions. Moreover, the gut

microbiota plays a protective role in the mouse model of DSS-induced mouse colitis (Le Bras, 2022). The antibiotic effects of azithromycin might kill the gut bacteria, leading to the loss of anti-inflammatory functions. Rolipram mildly improved the colon length but could not bring remarkable benefits. Importantly, pentamidine exhibited the best anti-inflammatory effects in ulcerative colitis. Although pentamidine moderately affects IFN- γ -induced NO production *in vitro*, it might target a broad spectrum of pro-inflammatory mediators *in vivo* with efficient bioavailability. Followed by pentamidine, auranofin also remarkably ameliorated ulcerative colitis, as expected from the *in vitro* studies. These effects might be attributed to the auranofin's NF-kB pathway inhibitory property (Atreya et al., 2008; Hwangbo et al., 2021). In conclusion, auranofin consistently performed as a potent inhibitor of IFN- γ -induced NO production and in colitis pathogenesis.

Sepsis is a potentially life-threatening medical condition that occurs when the body's response to infection becomes dysregulated and causes inflammation. It is a major concern in hospitals. Globally, 48.9 million sepsis incidences and 11 million deaths occur yearly, accounting for 19.7% of all global deaths (Hotchkiss et al., 2016; Rudd et al., 2020). It can occur due to any infection, including bacterial, viral, or fungal. The signs of sepsis involve cytokine storm, hemolysis, coagulation, and vascular leakage. A study on the extended prevalence of infection and related sepsis in intensive care unit patients found that 62% of the positive isolates from patients were Gram-negative organisms (Vincent et al., 2009). Previously, we extensively characterized the effect of NOS2 in a mouse model of the Gram-negative pathogen *Salmonella* Typhimurium infection-induced sepsis. We found that NOS2-induced NO production is essential for the survival of mice (Yadav et al., 2018). NO is enhanced during sepsis in patients but the effects of NO donors and inhibitors are often inconsistent in clinical reports (Yadav et al., 2019). In this study, we tested the efficacy of pentamidine and auranofin in a mouse model of the Gram-negative pathogen *Salmonella* Typhimurium infection-induced sepsis. The administration of pentamidine and auranofin was performed 3-4 hours post-infection to resemble the clinical scenario. With a single administration, both compounds alleviated sepsis pathogenesis by significantly extending survival. Most likely, the survival of mice in this model is due to the potent anti-inflammatory effects of these two compounds. Many pro-inflammatory cytokines, including IFN- γ *in vivo*, likely contribute to NO production by NOS2 in ulcerative colitis and sepsis (Soufli et al., 2016; Yadav et al., 2018; Pathak et al., 2021). Our studies involving *Nos2*^{-/-} mice demonstrated that NO

production by NOS2 contributes to the disease pathogenesis in DSS-induced ulcerative colitis and *Salmonella* Typhimurium-induced sepsis in mice (Fig.14) (Yadav et al., 2018; Pathak et al., 2021). The serum level of IFN- γ increases in both the preclinical mouse disease models (Yadav et al., 2018; Pathak et al., 2021). Mechanistically, the anti-inflammatory effects of pentamidine and auranofin in ulcerative colitis and sepsis *in vivo* may reduce multiple pro-inflammatory signaling processes. Importantly, pentamidine and auranofin lower inflammatory responses in two distinct mice models of inflammatory disease.

Impact

The model and method of high-throughput screening on IFN- γ -activated H6 cells and the systematic compound validation approach applied and depicted here is paramount in identifying novel and better immunomodulatory drugs targeting many inflammatory diseases. The novel leads identified here against IFN- γ -induced NO production process can be therapeutically repurposed to mitigate adverse inflammatory disease pathogenesis. Furthermore, auranofin and pentamidine may serve as therapeutic options in alternative or combinatorial regimens to treat the chronic inflammatory conditions of inflammatory diseases.

Highlights and future directions

Novel highlights

1. The screening against IFN- γ signaling induced NO production was Novel.
2. All the hit compounds are potent inhibitors of IFN- γ -induced NO and ROS production.
3. The effects of hit compounds are not global, instead specific for NO-dependent arms.
4. Auranofin is effective against IFN- γ -induced NO and IL6 production in resident and TG-elicited PMs.
5. Auranofin and pentamidine improved disease pathogenesis in DSS-induced colitis and *Salmonella* Typhimurium-induced sepsis.
6. Auranofin and pentamidine synergize in protection against DSS-induced colitis.

Future directions

1. Detailed mechanistic investigation of the specific targets of the lead compounds.
2. Identify the protective effects of auranofin and pentamidine in other IFN- γ -NO-axis-dominated inflammatory diseases.
3. Clinical trials in patients with colitis and sepsis for approval.

Remarks:

a. The authors of this research are: Avik Chattopadhyay^a (Lead student investigator), Joel P. Joseph^b, Sirisha Jagdish^a, Somak Chaudhuri^a, Nikita S. Ramteke^a, Aagosh Kishore Karhale^a, Uchenna Waturuocha^c, Prof. Deepak Kumar Saini^{b,c}, and Prof. Dipankar Nandi^a (Principal Investigator).

[^aDepartment of Biochemistry, Indian Institute of Science, Bangalore 560012, India

^bCentre for BioSystems Science and Engineering, Indian Institute of Science, Bangalore 560012, India

^cDepartment of Developmental Biology and Genetics, Indian Institute of Science, Bangalore 560012, India]

b. We greatly appreciate the support from the members of the Divisional flow cytometry facility and Central Animal Facility, IISc. This study was funded by SERB grant CRG/2021/004284, core grants from IISc and the DBT- IISc partnership program. In addition, the infrastructural support from DST-FIST to the Department of Biochemistry, IISc is greatly appreciated. In addition, the support from all members of the laboratory is greatly appreciated.

References

- Alspach E, Lussier DM, Schreiber RD (2019) Interferon γ and its important roles in promoting and inhibiting spontaneous and therapeutic cancer immunity. *Cold Spring Harb Perspect Biol* 11:a028480
- Ambs S, Merriam WG, Bennett WP, et al (1998) Frequent nitric oxide synthase-2 expression in human colon adenomas: implication for tumor angiogenesis and colon cancer progression. *Cancer Res* 58:334–341
- Antoniou E, Margonis GA, Angelou A, et al (2016) The TNBS-induced colitis animal model: An overview. *Annals of medicine and surgery* 11:9–15
- Arellano G, Ottum PA, Reyes LI, et al (2015) Stage-specific role of interferon-gamma in experimental autoimmune encephalomyelitis and multiple sclerosis. *Front Immunol* 6:492
- Atreya I, Atreya R, Neurath MF (2008) NF- κ B in inflammatory bowel disease. *J Intern Med* 263:591–596
- Ayers M, Lunceford J, Nebozhyn M, et al (2017) IFN- γ -related mRNA profile predicts clinical response to PD-1 blockade. *J Clin Invest* 127:2930–2940
- Barnes PJ (2006) How corticosteroids control inflammation: quintiles prize lecture 2005. *Br J Pharmacol* 148:245–254
- Benchabane S, Boudjelida A, Toumi R, et al (2016) A case for IL-6, IL-17A, and nitric oxide in the pathophysiology of Sjögren's syndrome. *Int J Immunopathol Pharmacol* 29:386–397
- Blanchette J, Jaramillo M, Olivier M (2003) Signalling events involved in interferon- γ -inducible macrophage nitric oxide generation. *Immunology* 108:513–522
- Bogdan C (2015) Nitric oxide synthase in innate and adaptive immunity: an update. *Trends Immunol* 36:161–178
- Braverman J, Stanley SA (2017) Nitric oxide modulates macrophage responses to *Mycobacterium tuberculosis* infection through activation of HIF-1 α and repression of NF- κ B. *The Journal of Immunology* 199:1805–1816
- Bustin SA, Beaulieu J-F, Huggett J, et al (2010) MIQE precis: Practical implementation of minimum standard guidelines for fluorescence-based quantitative real-time PCR experiments. *BMC Mol Biol* 11:1–5
- Chandrasekar BS, Yadav S, Victor ES, et al (2015) Interferon-gamma and nitric oxide synthase 2 mediate the aggregation of resident adherent peritoneal exudate cells: implications for the host response to pathogens. *PLoS One* 10:e0128301
- Chattopadhyay A, Joseph JP, Shyam S, Nandi D (2022) Characterizing *Salmonella* Typhimurium-induced Septic Peritonitis in Mice. *JoVE (Journal of Visualized Experiments)* e63695

- Coates E, Barr A, Totton N, et al (2021) P97 Management of steroid resistant ulcerative colitis—a national survey of UK practice
- Dell RB, Holleran S, Ramakrishnan R (2002) Sample size determination. *ILAR J* 43:207–213
- Dey P, Panga V, Raghunathan S (2016) A cytokine signalling network for the regulation of inducible nitric oxide synthase expression in rheumatoid arthritis. *PLoS One* 11:e0161306
- Doan T, Massarotti E (2005) Rheumatoid arthritis: an overview of new and emerging therapies. *The Journal of Clinical Pharmacology* 45:751–762
- Esposito G, Capoccia E, Sarnelli G, et al (2012) The antiprotozoal drug pentamidine ameliorates experimentally induced acute colitis in mice. *J Neuroinflammation* 9:1–12
- Gao J, Shi LZ, Zhao H, et al (2016) Loss of IFN- γ pathway genes in tumor cells as a mechanism of resistance to anti-CTLA-4 therapy. *Cell* 167:397–404
- Ghosn EEB, Cassado AA, Govoni GR, et al (2010) Two physically, functionally, and developmentally distinct peritoneal macrophage subsets. *Proceedings of the National Academy of Sciences* 107:2568–2573
- Gil-Moles M, Basu U, Büssing R, et al (2020) Gold metallodrugs to target coronavirus proteins: inhibitory effects on the spike-ACE2 interaction and on PLpro protease activity by auranofin and gold organometallics. *Chemistry—A European Journal* 26:15140–15144
- Granados-Principal S, Liu Y, Guevara ML, et al (2015) Inhibition of iNOS as a novel effective targeted therapy against triple-negative breast cancer. *Breast cancer research* 17:1–16
- Han S, Kim K, Kim H, et al (2008) Auranofin inhibits overproduction of pro-inflammatory cytokines, cyclooxygenase expression and PGE 2 production in macrophages. *Arch Pharm Res* 31:67–74
- Herbst S, Schaible UE, Schneider BE (2011) Interferon gamma activated macrophages kill mycobacteria by nitric oxide induced apoptosis. *PLoS One* 6:e19105
- Hong L, Ye L (2022) The interferon- γ receptor pathway: a new way to regulate CAR T cell-solid tumor cell adhesion. *Signal Transduct Target Ther* 7:315
- Hotchkiss RS, Moldawer LL, Opal SM, et al (2016) Sepsis and septic shock. *Nat Rev Dis Primers* 2:1-21
- Hu X, Li J, Fu M, et al (2021) The JAK/STAT signaling pathway: from bench to clinic. *Signal Transduct Target Ther* 6:402
- Hu X, Li W-P, Meng C, Ivashkiv LB (2003) Inhibition of IFN- γ signaling by glucocorticoids. *The journal of immunology* 170:4833–4839
- Huang H, Xie M, Gao L, et al (2019) Rolipram, a PDE4 inhibitor, enhances the inotropic effect of rat heart by activating SERCA2a. *Front Pharmacol* 10:221
- Hwangbo H, Ji SY, Kim MY, et al (2021) Anti-inflammatory effect of auranofin on palmitic acid and LPS-induced inflammatory response by modulating TLR4 and NOX4-mediated NF- κ B signaling pathway in RAW264. 7 macrophages. *Int J Mol Sci* 22:5920

- Ignarro LJ (2019) Nitric oxide is not just blowing in the wind. *Br J Pharmacol* 176:131
- Ito R, Shin-Ya M, Kishida T, et al (2006) Interferon-gamma is causatively involved in experimental inflammatory bowel disease in mice. *Clin Exp Immunol* 146:330–338
- Ivashkiv LB (2018) IFN γ : signalling, epigenetics and roles in immunity, metabolism, disease and cancer immunotherapy. *Nat Rev Immunol* 18:545–558
- Jones G-R, Bain CC, Fenton TM, et al (2018) Dynamics of colon monocyte and macrophage activation during colitis. *Front Immunol* 9:2764
- Kak G, Raza M, Tiwari BK (2018) Interferon-gamma (IFN- γ): Exploring its implications in infectious diseases. *Biomol Concepts* 9:64–79
- Kann O, Almouhanna F, Chausse B (2022) Interferon γ : A master cytokine in microglia-mediated neural network dysfunction and neurodegeneration. *Trends Neurosci*
- Kleinert H, Art J, Pautz A (2010) Chapter 7–Regulation of the Expression of Inducible Nitric Oxide Synthase. *Nitric Oxide (Second Edition)*, in: LJ Ignarro (Ed) Academic Press, San Diego 211–267
- Kotredes KP, Gamero AM (2013) Interferons as inducers of apoptosis in malignant cells. *Journal of Interferon & Cytokine Research* 33:162–170
- Lakatos PL, Lakatos L (2008) Risk for colorectal cancer in ulcerative colitis: changes, causes and management strategies. *World journal of gastroenterology: WJG* 14:3937
- Langer V, Vivi E, Regensburger D, et al (2019) IFN- γ drives inflammatory bowel disease pathogenesis through VE-cadherin–directed vascular barrier disruption. *J Clin Invest* 129:4691–4707
- Lee SH, Kwon JY, Kim S-Y, et al (2017) Interferon-gamma regulates inflammatory cell death by targeting necroptosis in experimental autoimmune arthritis. *Sci Rep* 7:10133
- Liu L, Wang Y, Fan Y, et al (2004) IFN- γ activates cAMP/PKA/CREB signaling pathway in murine peritoneal macrophages. *Journal of interferon & cytokine research* 24:334–342
- Liu W, Zhang S, Wang J (2022) IFN- γ , should not be ignored in SLE. *Front Immunol* 13:954706
- Lu G, Zhang R, Geng S, et al (2015) Myeloid cell-derived inducible nitric oxide synthase suppresses M1 macrophage polarization. *Nat Commun* 6:6676
- Malu S, Srinivasan S, Maiti PK, et al (2003) IFN- γ bioassay: development of a sensitive method by measuring nitric oxide production by peritoneal exudate cells from C57BL/6 mice. *J Immunol Methods* 272:55–65
- Martin E, Nathan C, Xie QW (1994) Role of interferon regulatory factor 1 in induction of nitric oxide synthase. *J Exp Med* 180:977–984
- Neurath MF (2014) Cytokines in inflammatory bowel disease. *Nat Rev Immunol* 14:329–342
- Okayama H, Saito M, Oue N, et al (2013) NOS2 enhances KRAS-induced lung carcinogenesis, inflammation and microRNA-21 expression. *Int J Cancer* 132:9–18

- Park YH, Kim N, Shim YK, et al (2015) Adequate dextran sodium sulfate-induced colitis model in mice and effective outcome measurement method. *J Cancer Prev* 20:260
- Pathak S, Gokhroo A, Dubey AK, et al (2021) 7-Hydroxy Frullanolide, a sesquiterpene lactone, increases intracellular calcium amounts, lowers CD4⁺ T cell and macrophage responses, and ameliorates DSS-induced colitis. *Int Immunopharmacol* 97:107655
- Polat G, Ugan RA, Cadirci E, Halici Z (2017) Sepsis and septic shock: current treatment strategies and new approaches. *Eurasian J Med* 49:53
- Prasanna SJ, Saha B, Nandi D (2007) Involvement of oxidative and nitrosative stress in modulation of gene expression and functional responses by IFN γ . *Int Immunol* 19:867–879
- Principi N, Blasi F, Esposito S (2015) Azithromycin use in patients with cystic fibrosis. *European Journal of Clinical Microbiology & Infectious Diseases* 34:1071–1079
- Rafa H, Amri M, Saoula H, et al (2010) Involvement of interferon- γ in bowel disease pathogenesis by nitric oxide pathway: a study in Algerian patients. *Journal of Interferon & Cytokine Research* 30:691–697
- Rakshit S, Chandrasekar BS, Saha B, et al (2014) Interferon-gamma induced cell death: Regulation and contributions of nitric oxide, cJun N-terminal kinase, reactive oxygen species and peroxynitrite. *Biochim Biophys Acta Mol Cell Res* 1843:2645–2661.
<https://doi.org/10.1016/j.bbamcr.2014.06.014>
- Ray S, Da Costa R, Das M, Nandi D (2019) Interplay of cold shock protein E with an uncharacterized protein, YciF, lowers porin expression and enhances bile resistance in *Salmonella Typhimurium*. *Journal of Biological Chemistry* 294:9084–9099
- Roder C, Thomson MJ (2015) Auranofin: repurposing an old drug for a golden new age. *Drugs R D* 15:13–20
- Romero CR, Herzig DS, Etogo A, et al (2010) The role of interferon- γ in the pathogenesis of acute intra-abdominal sepsis. *J Leukoc Biol* 88:725–735
- Rudd KE, Johnson SC, Agesa KM, et al (2020) Global, regional, and national sepsis incidence and mortality, 1990–2017: analysis for the Global Burden of Disease Study. *The Lancet* 395:200–211
- Saha B, Prasanna SJ, Chandrasekar B, Nandi D (2010) Gene modulation and immunoregulatory roles of Interferon γ . *Cytokine* 50:1–14
- Salamone FR, Cunha BA (1988) Update on pentamidine for the treatment of *Pneumocystis carinii* pneumonia. *Clin Pharm* 7:501–510
- Shintani N, Nakajima T, Okamoto T, et al (1998) Involvement of CD4⁺ T cells in the development of dextran sulfate sodium-induced experimental colitis and suppressive effect of IgG on their action. *General Pharmacology: The Vascular System* 31:477–481
- Soufli I, Toumi R, Rafa H, Touil-Boukoffa C (2016) Overview of cytokines and nitric oxide involvement in immuno-pathogenesis of inflammatory bowel diseases. *World J Gastrointest Pharmacol Ther* 7:353

Su Q, Wang F, Dong Z, et al (2020) IFN γ induces apoptosis in human melanocytes by activating the JAK1/STAT1 signaling pathway. *Mol Med Rep* 22:3111–3116

Sultana J, Cutroneo PM, Crisafulli S, et al (2020) Azithromycin in COVID-19 patients: pharmacological mechanism, clinical evidence and prescribing guidelines. *Drug Saf* 43:691–698

Sun T, Zhang Y (2008) Pentamidine binds to tRNA through non-specific hydrophobic interactions and inhibits aminoacylation and translation. *Nucleic Acids Res* 36:1654–1664

Svec D, Tichopad A, Novosadova V, et al (2015) How good is a PCR efficiency estimate: Recommendations for precise and robust qPCR efficiency assessments. *Biomol Detect Quantif* 3:9–16

Taylor SC, Mrkusich EM (2014) The state of RT-quantitative PCR: firsthand observations of implementation of minimum information for the publication of quantitative real-time PCR experiments (MIQE). *Microb Physiol* 24:46–52

Truett, G. "e., Heeger, P., Mynatt, R. l., Truett." A. a., Walker, J. a., Warman, M. l (2000): 52-54

Vincent J-L, Rello J, Marshall J, et al (2009) International study of the prevalence and outcomes of infection in intensive care units. *JAMA* 302:2323–2329

Warner TD, McCartney SA (1998) NOS inhibitors in colitis: a suitable case for treatment? *Gut* 42:152–153

Yadav S, Pathak S, Sarikhani M, et al (2018) Nitric oxide synthase 2 enhances the survival of mice during *Salmonella Typhimurium* infection-induced sepsis by increasing reactive oxygen species, inflammatory cytokines and recruitment of neutrophils to the peritoneal cavity. *Free Radic Biol Med* 116:73–87

Yadav S, Verma T, Pathak S, Nandi D (2019) Understanding the roles of nitric oxide during sepsis, an inflammatory disorder. *Therapeutic Application of Nitric Oxide in Cancer and Inflammatory Disorders* 243–276

Youn HS, Lee JY, Saitoh SI, et al (2006) Auranofin, as an anti-rheumatic gold compound, suppresses LPS-induced homodimerization of TLR4. *Biochem Biophys Res Commun* 350:866–871

Zaidi MR (2019) The interferon-gamma paradox in cancer. *Journal of Interferon & Cytokine Research* 39:30–38

Zhang J-H, Chung TD, Oldenburg KRJ (1999) *Biomol. Screen*, accepted for publication

Zhang X, Selvaraju K, Saei AA, et al (2019) Repurposing of auranofin: Thioredoxin reductase remains a primary target of the drug. *Biochimie* 162:46–54

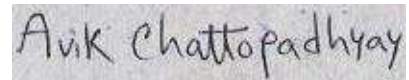
Zhang Y-Z, Li Y-Y (2014) Inflammatory bowel disease: pathogenesis. *World journal of gastroenterology: WJG* 20:91

Zou P, Chen M, Ji J, et al (2015) Auranofin induces apoptosis by ROS-mediated ER stress and mitochondrial dysfunction and displayed synergistic lethality with piperlongumine in gastric cancer. *Oncotarget* 6:36505

Declaration:

I hereby declare that the research work described here was performed by me as the lead student investigator.

Signature with date:

A handwritten signature in black ink on a light-colored background. The signature reads "Avik Chattopadhyay" in a cursive, slightly slanted script.

31-08-23